Research paper

Structure-guided optimization of 3-hydroxybenzoisoxazole derivatives as inhibitors of Aldo-keto reductase 1C3 (AKR1C3) to target prostate cancer

Agnese Chiara Pippione [a,1], Sandra Kovachka [a,b,1], Chiara Vigato [a], Laura Bertarini [a,c], Iole Mannella [a], Stefano Sainas [a], Barbara Rolando [a], Enrica Denasio [d], Helen Piercy-Mycock [d], Linda Romalho [e], Edoardo Salladini [a], Salvatore Adinolfi [a], Daniele Zonari [a], Caterina Peraldo-Neia [f], Giovanna Chiorino [f], Alice Passoni [g], Osman Asghar Mirza [e], Karla Frydenvang [e], Klaus Pors [d], Marco Lucio Lolli [a], Francesca Spyrakis [a], Simonetta Oliaro-Bosso [a,**], Donatella Boschi [a,*]

[a] Department of Science and Drug Technology, University of Turin, via Pietro Giuria 9, 10125, Turin, Italy
[b] The Herbert Wertheim UF Scripps Institute for Biomedical Innovation & Technology, Jupiter, FL, USA
[c] Department of Life Sciences, University of Modena and Reggio Emilia, via Campi 103, 41125, Modena, Italy
[d] Institute of Cancer Therapeutics, Faculty of Life Sciences, University of Bradford, West Yorkshire, BD7 1DP, UK
[e] Department of Drug Design and Pharmacology, University of Copenhagen, Jagtvej 162, DK-2100, Copenhagen, Denmark
[f] Laboratory of Cancer Genomics, Fondazione Edo ed Elvo Tempia, via Malta 3, 13900, Biella, Italy
[g] Department of Environmental Health Sciences, Istituto di Ricerche Farmacologiche Mario Negri IRCCS, Via Mario Negri 2, 20156, Milan, Italy

ABSTRACT

AKR1C3 is an enzyme that is overexpressed in several types of radiotherapy- and chemotherapy-resistant cancers. Despite AKR1C3 is a validated target for drug development, no inhibitor has been approved for clinical use. In this manuscript, we describe our study of a new series of potent AKR1C3-targeting 3-hydroxybenzoisoxazole based inhibitors that display high selectivity over the AKR1C2 isoform and low micromolar activity in inhibiting 22Rv1 prostate cancer cell proliferation. *In silico* studies suggested proper substituents to increase compound potency and provided with a mechanistic explanation that could clarify their different activity, later confirmed by X-ray crystallography. Both the *in-silico* studies and the crystallographic data highlight the importance of 90° rotation around the single bond of the biphenyl group, in ensuring that the inhibitor can adopt the optimal binding mode within the active pocket. The *p*-biphenyls that bear the *meta*-methoxy, and the *ortho*- and *meta*-trifluoromethyl substituents (in compounds **6a**, **6e** and **6f** respectively) proved to be the best contributors to cellular potency as they provided the best IC_{50} values in series (2.3, 2.0 and 2.4 μM respectively) and showed no toxicity towards human MRC-5 cells. Co-treatment with scalar dilutions of either compound **6** or **6e** and the clinically used drug abiraterone led to a significant reduction in cell proliferation, and thus confirmed that treatment with both CYP171A1-and AKR1C3-targeting compounds possess the potential to intervene in key steps in the steroidogenic pathway. Taken together, the novel compounds display desirable biochemical potency and cellular target inhibition as well as good *in-vitro* ADME properties, which highlight their potential for further preclinical studies.

1. Introduction

Aldo-keto reductase 1C (AKR1C) is a superfamily that contains four highly homologous isoforms (AKR1C1-AKR1C4) with diverse biological functions [1]. The cytosolic member AKR1C3 plays a crucial role in the reduction of a broad spectrum of both physiological and xenobiotic substrates [2]. AKR1C3 is known to regulate the local concentration of ligands that are available for nuclear receptors, as well as the reduction

of the 17-ketosteroid function of Δ4-androstene-3,17-dione and 5α-androstane-3,17-dione to testosterone and 5α-dihydrotestosterone (DHT), respectively. As both testosterone and DHT are potent androgens with a high affinity for the androgen receptor (AR), AKR1C3 plays an important role in the steroidogenic pathway in ensuring effective androgen generation for subsequent AR binding. Similarly, it reduces estrone and progesterone to 17β-estradiol and 20α-hydroxyprogesterone, respectively, by regulating their affinities towards both the estrogen receptor (ER) and the progesterone receptor (PR) [2]. AKR1C3 also acts as a prostaglandin (PG) F2 synthase, regulating cell proliferation and differentiation [2]. Furthermore, AKR1C3 can act as a phase-I biotransformation enzyme that reduces endogenous reactive ketone and aldehyde metabolites as well as a variety of exogenous compounds, including drugs. Its function is important in detoxifying and facilitating the excretion of metabolites and drugs, although it also contributes to chemoresistance [2]. AKR1C3 has also been therapeutically targeted via its capacity to bioreduce NO_2-containing prodrugs [3,4]. Accordingly, overexpressed AKR1C3 in tumor tissue is considered a valid target for both inhibitor and prodrug development as a means to dose-intensify cancer tissues whilst reducing systemic exposure [5]. While the greatest amount of focus has been paid to AKR1C3 expression in prostate cancer [6], emerging knowledge has highlighted expression in other cancer types, including breast cancer [7], non-small cell lung cancer (NSCLC) [8], esophageal cancer [9,10], liver cancer [11,12], and leukaemia [13], with roles linked to tumor invasiveness, aggressiveness and resistance to chemotherapy and radiation therapy [14,15]. Unfortunately, more recently approved therapies for castration-resistant prostate cancer (CRPC), such as enzalutamide (ENZA) and (ABI), also suffer from drug resistance, which emerges within months of treatment. AKR1C3 overexpression leads to the production of intratumoral androgens [16], which can be partially prevented via the co-administration of indomethacin (INDO), a weak and poorly selective AKR1C3 inhibitor [16–19], or more selective AKR1C3 inhibitors [20]. It has recently been demonstrated that AKR1C3 also mediates the inactivation of, and resistance to, doxorubicin, and other anthracyclines [21,22], via the carbonyl reductase activity of the enzyme. AKR1C3 knockdown has been observed to significantly enhance the sensitivity of hepatocellular

carcinoma cells to ferroptosis inducers, which thus identifies AKR1C3 as having a role in ferroptosis. This observation also emphasizes how AKR1C3 is a possible therapeutic target with which to improve the effectiveness of ferroptosis-based antitumor therapy [23]. Several small-molecule inhibitors have been reported to potently inhibit the activity of AKR1C3 (interesting and extensive reviews describe their discovery [24,25]), and two have entered clinical trials (Fig. 1a: ASP9521, NTC01352208 for CRPC and BAY-1128688 [26], NCT03373422 for endometriosis). Although no AKR1C3 inhibitor has been approved for clinical use to date, there is substantial evidence to support the enzyme as a target for drug development.

In order to improve the bioavailability of carboxylic acid derivatives and circumvent their transporter-mediated uptake [27,28], we have recently applied scaffold-hopping and bioisosteric replacement techniques to the structure of two NSAIDs, INDO [29] and flufenamic acid (FLU) [30–32], with the purpose of developing new AKR1C3 inhibitors. Replacing the benzoic acid moiety of FLU with the acidic hydroxyazolecarbonylic scaffold (Fig. 1) allowed us to obtain compound **1** (Fig. 1), which has a minor off-target effect on AKR1C2 and cyclooxygenases (COX1 and 2) [30]. Novel N-substituted hydroxylated triazoles with high selectivity (higher than 1500-fold) for the C3, over the C2, isoform were successively developed (compound **1a**, Fig. 1) using a combination of X-ray structural studies, computational design and iterative rounds of synthesis and biological evaluation [32]. The application of a conformational restriction approach on FLU led to a focused library of 3-hydroxybenzoisoxazole-based compounds, of which 4-(3, 5-bis-trifluoromethylphenyl)-3-hydroxybenzoisoxazole exhibited the best AKR1C3 inhibitory activity and selectivity (compound **2**, Fig. 1) [31]. The crystal structure of AKR1C3 in complex with **1** and **2** [31], in combination with molecular-docking studies, has guided the design of the new 3-hydroxybenzoisoxazole-based compounds. We here describe the structure-based lead optimization that has led to new potent and selective AKR1C3 inhibitors. We will also present the synthesis employed to obtain the new compounds as well as their *in vitro* AKR1C3 inhibition by biochemical and cell-based assays alone and in combination with ABI. Finally, we report the binding mode of the most soluble compound **6b**, in the form of the high-resolution crystal structure of the
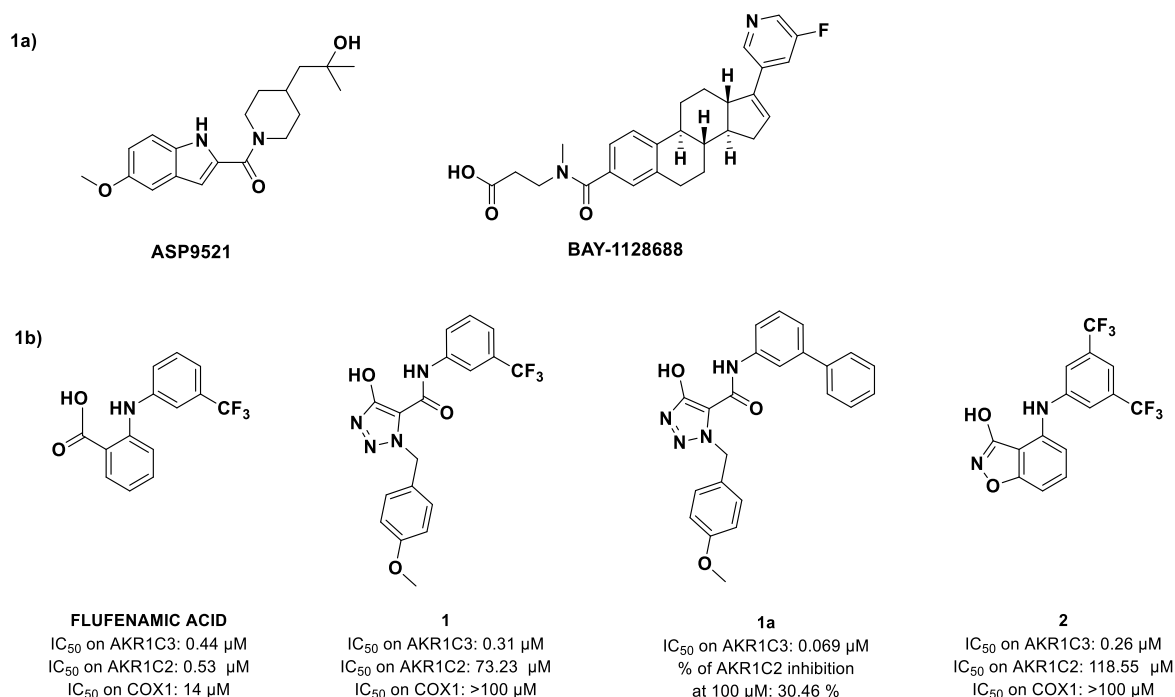

Fig. 1. Chemical structures of some AKR1C3 inhibitors: **a)** AKR1C3 inhibitors evaluated for clinical trials. **b)** AKR1C3 inhibitors previously proposed by the authors.

AKR1C3 in complex with **6b**.

2. Results and discussion

2.1. In-silico guided design of new 3-hydroxybenzoisoxazole-based inhibitors

Hydroxyazole derivatives are deprotonated at physiological pH and are good isosteres of the carboxylic function [33,34], and, indeed, all simulations were performed using the compounds in their ionized form. The design of this new series of 3-hydroxybenzoisoxazole-based inhibitors was performed starting with the crystallographic structure of AKR1C3 complexed with the previously published compound **2** (PDB ID 6F78 [31], Figs. 1 and 2), which was essential to pinpointing the characteristic compartments of the binding pocket and the crucial residues involved in ligand binding. As previously reported, the AKR1C3 binding site is delimited by five compartments: an oxyanion site (OS), formed by the cofactor NADP$^+$ and the catalytic residues Tyr55 and His117; a steroid channel (SC, Tyr24, Leu54, Ser129, Trp227) and three sub-pockets - SP1 (Ser118, Asn167, Tyr216, Phe306, Tyr319), SP2 (Trp86, Leu122, Ser129, Phe311) and SP3 (Tyr24, Glu192, Ser221, Tyr305) [35,36]. Compound **2** occupies the OS cavity to establish key interactions, via H-bonding, to Tyr55, His117 and NADP$^+$ and, via π-π stacking, with Tyr24, Trp227, Phe306 and NADP$^+$, which mediates an additional π-π interaction with Tyr216. Furthermore, the 3,5-trifluoromethylphenyl moiety is located in the SP1 cavity, which orients one trifluoromethyl towards the deepest part of SP1, while placing the other close to the Phe311 in SP2 (Fig. 2a) [31]. We designed this new series of compounds to better occupy SP1 and SP2, and potentially increase both affinity and activity. The applied docking procedure was validated by redocking the co-crystallized compound **2** inside the corresponding binding site. As shown in Fig. 2b we obtained docking pose superposed well with the crystallographic structure.

First, we replaced the 3,5-trifluoromethylphenyl moiety with bulkier groups (Fig. 3), as done in previous studies for other compound series [31,32]. As predicted by docking simulations, all newly designed compounds placed the 3-hydroxybenzoisoxazole core in the OS cavity, which follows the orientation obtained from X-ray structures.

The introduction of a phenoxyphenyl substituent, as in compounds **3** and **4** (Fig. 3), allowed the formation of an additional polar interaction between Ser118 and the bridging oxygen of the ligand. The phenyl moiety formed hydrophobic and π-π stacking contact with residues in either the SP1 sites, depending on whether the ring was substituted in the *meta* or *para* position, respectively. The addition of a methoxy or hydroxy group to compound **4**, as in **4a** and **4b** respectively, generated steric clashes and a loss of stabilizing hydrophobic contact, thus explains

the non-conservation of poses during docking simulations, with the substituents alternating between filling SP1 and SP2.

A *meta* or *para* biphenyl moiety was inserted in compounds **5** and **6**, respectively. For compound **5** it was difficult to determine a preferred binding pose as the biphenyl group alternated between occupying SP1 and SP2, suggesting a lack of stable interaction. In contrast, compound **6** showed a highly conserved pose with the aromatic substituent being oriented towards SP2 (Fig. 4a). The flexibility around the single bond of the biphenyl system [37,38] resulted in a 60° rotated-orientation of the two rings, allowing the formation of π-π stacking and hydrophobic interactions with the surrounding residues.

The distal phenyl ring of compound **5** was then either methoxylated or hydroxylated at different positions, generating compounds **5a** and **5b** when the substitution occurred in the *meta* position, and compounds **5c** and **5d** when substituted in *para* position. When docked, the *meta*-substituted derivatives **5a** and **5b** were accommodated in SP1 and established polar contact with Tyr319. The presence of a hydroxyl group on **5b** allowed a H-bond network to form between Tyr319 and Tyr216, whereas this was not possible for **5a** due to oxygen methylation. Conversely, the *para*-substituted derivatives **5c** and **5d** oriented the biphenyl system towards SP2.

The aforementioned methoxy and hydroxy substituents were also introduced at the *meta* position of the second benzene ring of compound **6**, thus generating compounds **6a** and **6b**, respectively. Both derivatives followed the pose of compound **6**, with the biphenyl system able to rotate, fill SP2 and make good hydrophobic interactions. The introduction of a hydroxy group onto **6b** led to the formation of an additional H-bond with the side chain of Ser87 (Fig. 4b), while, for analogue **6a**, the presence of a bulkier methoxy group resulted in the rotation of the benzene ring, with the substituent pointing towards a contiguous hydrophobic site.

In view of the promising binding pose of compound **6**, we designed three trifluoromethyl-substituted derivatives to investigate whether the presence of a bulkier group may facilitate the improved occupation of SP1 and SP2. The trifluoromethyl substituent was introduced at the *ortho*, *meta* and *para* positions of the biphenyl moiety of compound **6**, thus generating **6e**, **6f**, **6g** respectively. Overall, the presence of a cumbersome group on the *ortho* (**6e**) and *para* (**6g**) positions had a similar effect on the rotation of the biphenyl system, orienting the two rings almost perpendicularly to each other. As previously mentioned, this orientation provided for optimal π-π and hydrophobic interactions between the ligand and the surrounding residues, as suggested by the low docking scores and highly conserved poses. The conformations assumed by **6e** and **6g** are highly superimposable with the single exception of the trifluoromethyl moiety, which is directed towards two different sites; in **6e**, it is accommodated in a hydrophobic site lined by
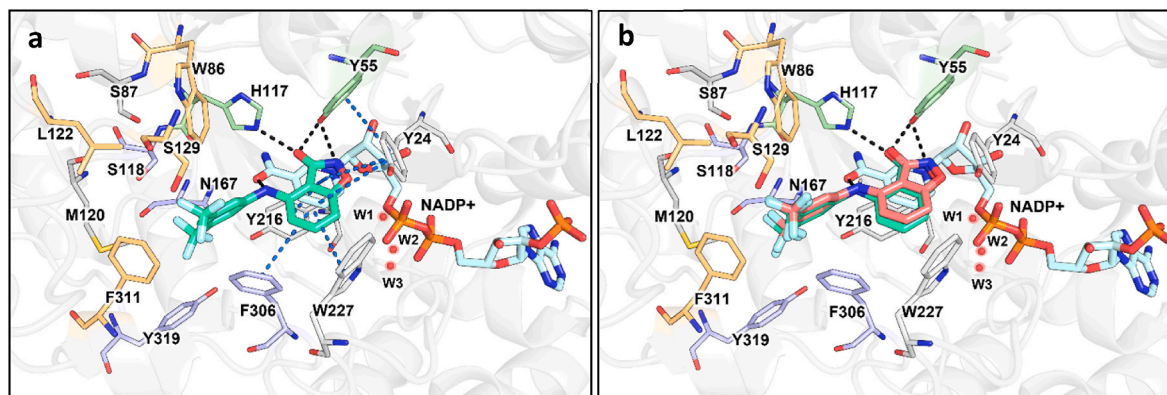

Fig. 2. a) X-ray pose of compound **2** (green) in AKR1C3 binding site (PDB ID 6F78). **b)** Superposition of the X-ray structure (green) with the docked pose (salmon) of compound **2**. The ligand and residues lining the pocket are shown as sticks. Residues are labeled and colored differently according to the sub-pockets they belong to (pale green: OS; light blue: SP1; light orange: SP2). The protein is shown as a gray transparent cartoon. Water molecules are shown as red spheres, hydrogen bonds as black dashed lines.

Fig. 3. Chemical structures of the 3-hydroxybenzoisoxazole-based AKR1C3 inhibitors studied in this work.

Fig. 4. Docking poses of (**a**) compound **6** (magenta) and (**b**) compound **6b** (cyan) in AKR1C3 binding site. The ligand and residues lining the pocket are shown as sticks. Residues are labeled and colored differently according to the sub-pockets they belong to (pale green: OS; light blue: SP1; light orange: SP2). The protein is shown as a gray transparent cartoon. Water molecules are shown as red spheres, hydrogen bonds as black dashed lines.
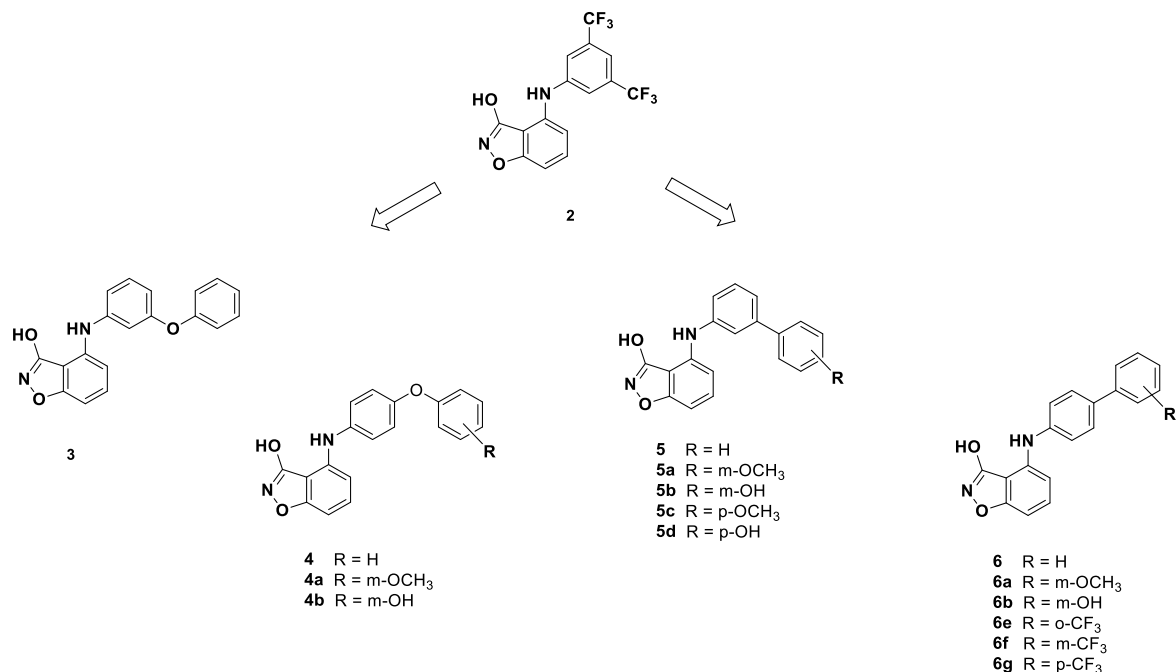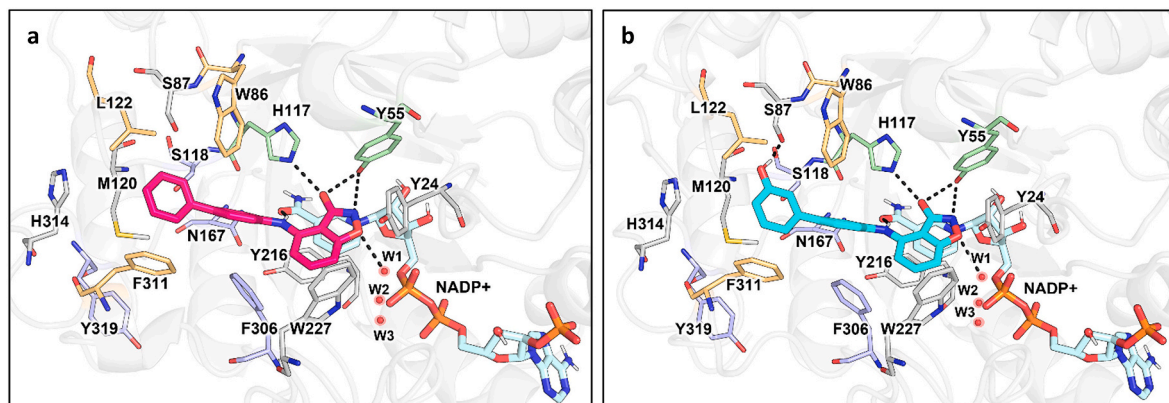
Phe306, Ser308 and Phe311 (Fig. 5a), while, in **6g**, it fills a deeper pocket bordered by Leu122, Val137, Phe139, Phe311 and His314 (Fig. 5b). Conversely, the introduction of a trifluoromethyl substituent in the *meta* position, as in compound **6f**, prevented the 90° rotation around the single bond of the biphenyl group, thus resulting in the benzene rings assuming a more planar orientation (dihedral angle: 27.9°) and in the occupation of a more external and solvent-accessible site (Fig. 5c).

Molecular-docking simulations seem to suggest that the proper occupation of the hydrophobic surface, belonging to SP1 and SP2, is critical to the ligand establishing a stable interaction with the enzyme active site. This high complementarity may be associated to higher affinity and to higher selectivity towards AKR1C3 compared to other isoforms.

2.2. Chemistry

Two different synthetic routes were followed to synthesize the benzoisoxazol-3-ol derivative target molecules for biological evaluation. For the synthesis of derivatives **3**–**6**, 4a–6a and 5c, we initially followed the scheme developed in our previous publication (Scheme 1) [31]. Briefly, we synthesized key intermediate **7**, which bears a benzo[d]isoxazol-3(2H)-one core protected by a trimethoxybenzyl moiety. Commercially available anilines **8a–8c**, **9a-9e** were coupled with **7** in a Buchwald-Hartwig reaction to obtain protected compounds **10a-10c** and **11a-11e**. The trimethoxybenzyl protective group was removed from **10a–10c** and **11a-11e** under mild conditions using triisopropylsilane and trifluoroacetic acid in DCM. A boron tribromide solution in DCM was used to convert the final methoxy-derivatives **4a**, **5a**, **5c** and **6a** into their corresponding hydroxy-derivatives **4b**, **5b**, **5d** and **6b**.

Scheme 1 was versatile and allowed several similar derivatives to be obtained. However, when the synthesis of key intermediate **7** needed to be scaled up to the multi-gram scale, several grams of the toxic reactant sodium cyanoborohydride were necessary in the first step of preparation [31]. Thus, we investigated a new synthetic scheme for a key intermediate that bears the 4-bromo-benzoisoxazol-3-ol moiety. Widlicka et al.,
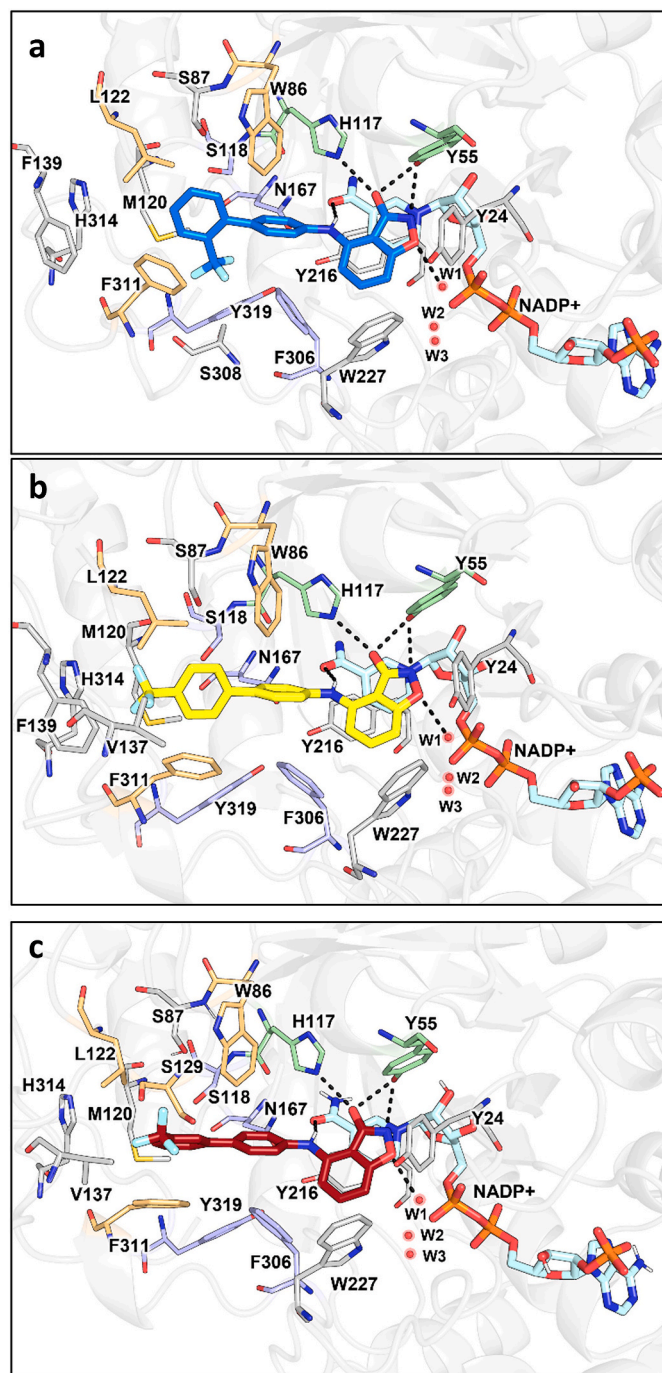
Fig. 5. Docking poses of compounds **6e** (**a**), **6g** (**b**) and **6f** (**c**) in the AKR1C3 binding site. The ligand and residues lining the pocket are shown as sticks. Residues are labeled and colored differently according to the sub-pockets they belong to (pale green: OS; light blue: SP1; light orange: SP2). The protein is shown as a gray transparent cartoon. Water molecules are shown as red spheres, hydrogen bonds as black dashed lines.

have described the multi-kg scale synthesis of 4-fluoro-3-hydroxybenzi-soxazole [39], starting from 2,6-difluorobenzoic acid, with good safety as well as atom economy. We employed this route, with some modifications, to prepare 4-bromobenzo[*d*]isoxazol-3-ol **14** (Scheme 2a). 2-bromo-6-fluorobenzoic acid **12** was converted to the corresponding acyl chloride using thionyl chloride and DMF in dry THF, and then treated with a solution of hydroxylamine, freshly prepared from hydroxylamine hydrochloride and potassium carbonate. After acidification, the desired hydroxamic acid **13** was recovered in pure form and in

high yields (91 % yield) upon the extraction of the reaction mixture with EtOAc, without further purification being required. Compound **13** was taken up in a concentrated aqueous solution of potassium hydroxide and heated to reflux to give complete conversion into **14**. Whereas the cyclization is very long (40 h in our case), as mentioned in the literature, the purification was easily performed via crystallization from acetonitrile, thus making the synthesis more amenable. Nonetheless, when we attempted to perform Buchwald-Hartwig amination on **14** we did not obtain the desired product. The reason for this failure was presumably the chelating ability of the 3-hydroxybenzoisoxazole core towards metal ions. Because this, we therefore decided to insert a protecting group to mask the hydroxyl function. After a failed attempt with Boc protection, we choose to proceed with the benzyl group for the synthesis of the *O*-benzyl protected compound **15a**. The reaction from **14** to **15a** also afforded regioisomer **15b**, due to the existing tautomeric equilibrium between 4-bromobenzo[*d*]isoxazol-3-ol and 4-bromobenzo[*d*]isoxazol-3(2H)-one. As previously reported [32,40], it is possible to regio-direct the benzylation towards the oxygen atom using silver oxide (Ag$_2$O). By applying this condition to **14**, we obtained **15a** and **15b** in a 5:1 ratio. Buchwald-Hartwig coupling conditions were then applied to *O*-benzylated 3-hydroxybenzoisoxazole **15a** in the presence of anilines **17a-c**. The latter were obtained via Suzuki coupling reactions between the corresponding boronic acids **16 a-c** and *para*-bromoaniline (Scheme 2b). The 3-benzyl groups of compounds **18a-c** were removed to give the deprotected hydroxyl moieties in trifluoroacetic acid at room temperature in the presence of the cationic scavenger thioanisole to give the final compounds **6e-g**.

Concluding, the second synthetic approach (Scheme 2a), used to prepare several compounds characterized by a 3-hydroxybenzoisoxazole core, offers some considerable advantages compared with the first synthetic approach (Scheme 1). Importantly, this protocol consists of only three linear steps for the synthesis of key intermediate **15a**, avoids the use of toxic sodium cyanoborohydride and displays higher atom economy. Interestingly, only one of the three steps involves the use of flash-chromatography as a purification technique, while less solvent-consuming purifications are utilized in the other two passages.

2.3. AKR1C3 and AKR1C2 inhibitor screening

The selective inhibition of the AKR1C3 enzyme, with respect to the C2 isoform, is considered fundamental for an effective anti-PC effect [25]. Since AKR1C2 is involved in the inactivation of DHT, its inhibition is undesirable, but the two isoforms share 86% sequence similarity. Accordingly, the inhibitory potencies of compounds **3-6g** were determined for both AKR1C2 and C3 and compared with those of ASP9521 [41], and **2** (Table 1). AKR1C2 and AKR1C1 share high sequence identity (97%) and any inhibitory effects against C2 will likely be recapitulated against C1, and the latter isoform was not included in the following experiments for this reason. On the other hand, AKR1C3 and C4 differ in terms of amino-acid sequence and binding-site structure, which lowers the probability that potent AKR1C3 inhibitors will also have an inhibitory effect on the AKR1C4 isoform. The following selectivity study therefore aims to quantify the C3 vs C2 selectivity ratio. The IC$_{50}$ and % of inhibition values reported in Table 1 were determined using recombinant purified enzymes, and by measuring S-tetralol oxidation in the presence of NADP$^+$. All of the new 3-hydroxybenzoisoxazole derivatives presented IC$_{50}$ values that were lower or similar to those of reference compound **2**. However, as they emit strong fluorescence signals at the 460 nm wavelength, the measurement of C2 inhibition at 100 μM was hampered. Therefore, the concentration was reduced to 1 μM (or, when possible, to 5 μM) and the inhibition rate was evaluated. It can be observed that the compounds have good selectivity to C3 over C2, suggesting, in accordance with previous studies, that the active site of the C3 isoform hosts the investigated substituents, such as the substituted *para*-diphenyl and *para*-phenoxyphenyl rings, whereas the C2 isoform accommodates these bulky substituents less easily. It can
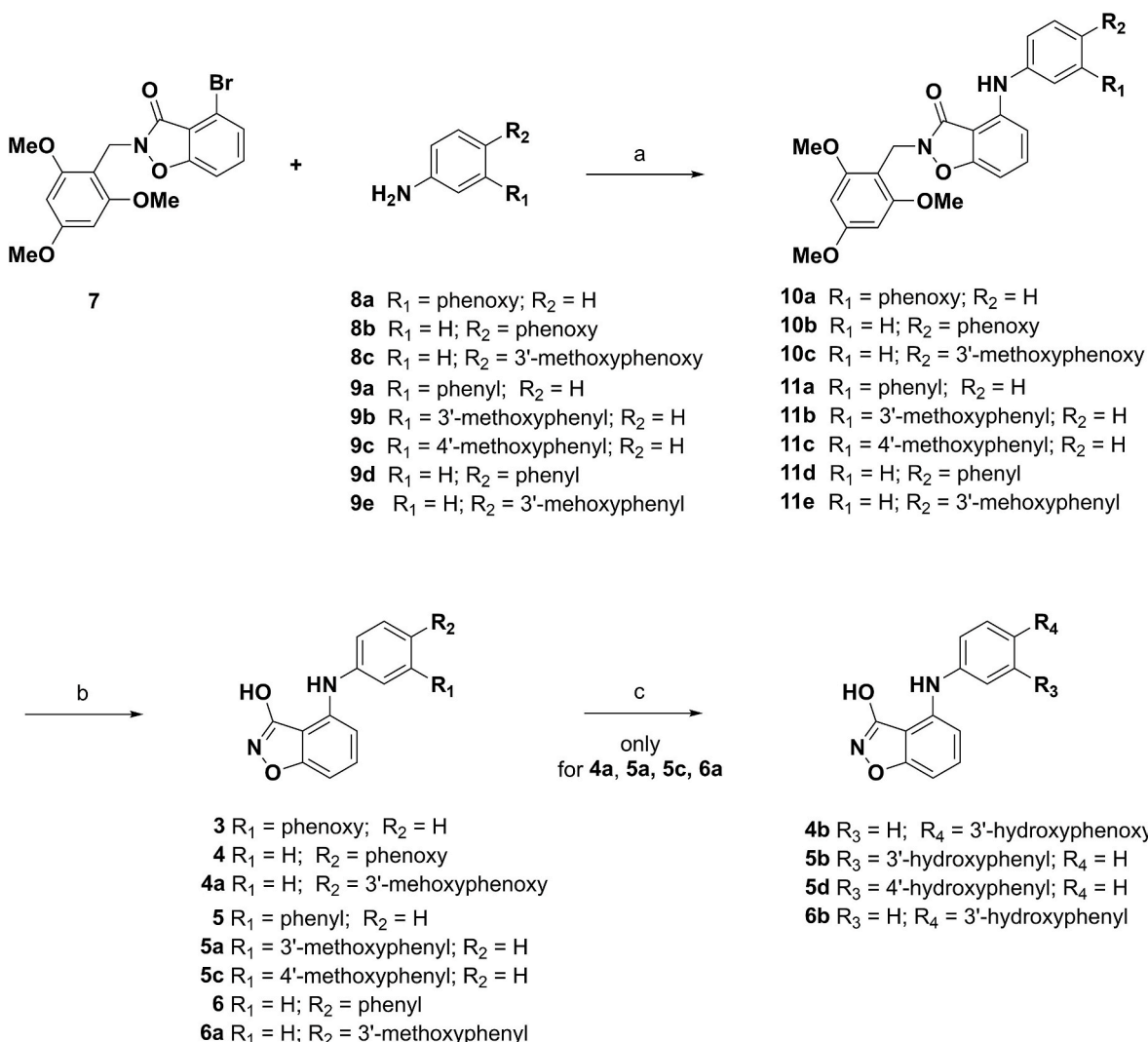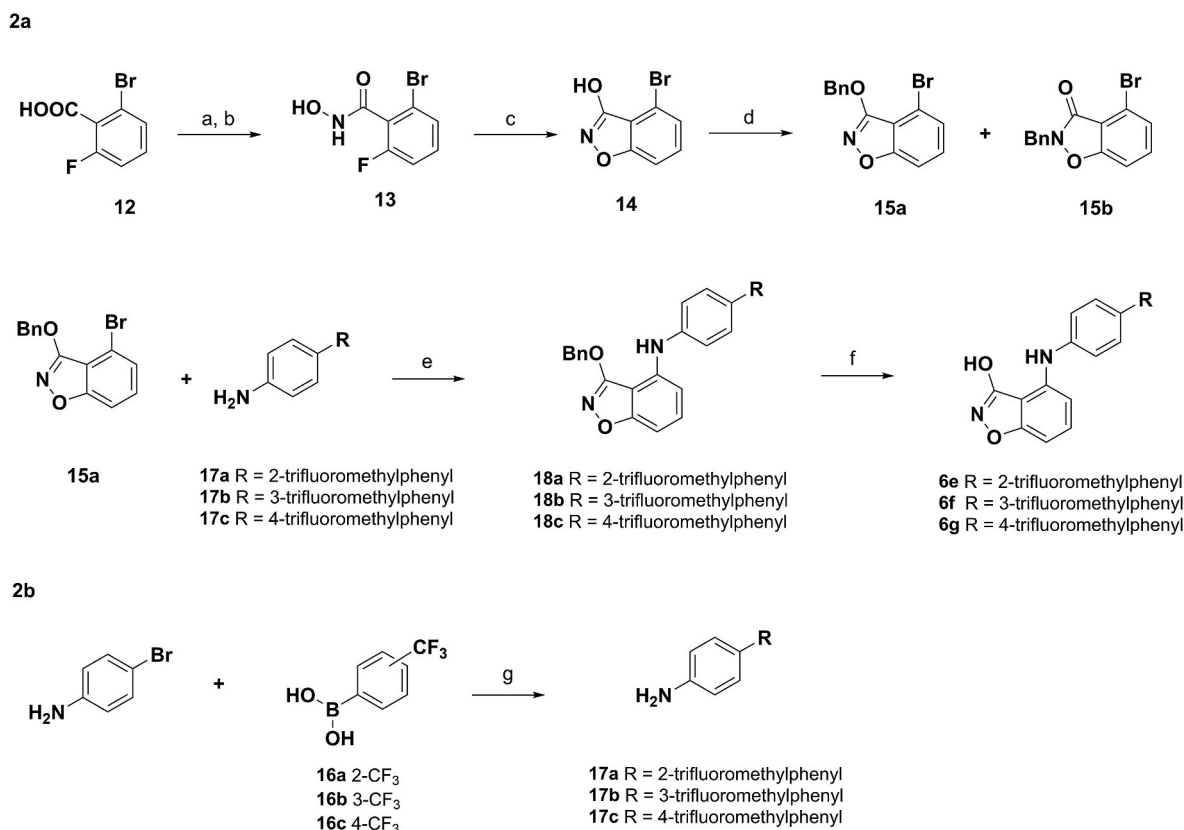
Scheme 1. Reagents and conditions: a) 5 mol% Pd(OAc)$_2$, 8 mol% BINAP, Cs$_2$CO$_3$, toluene, reflux, yield 53–93 %; b) TFA, (i-Pr)$_3$SiH, DCM, rt, yield 37–80 %; c) 1 M BBr$_3$ in DCM, DCM, 0 °C, then rt, yield 67–80 %.

be seen that the incorporation of a phenyl substituent at the *para* position of the aniline moiety (compound **6**) provided one of the most potent inhibitions (a 4-fold increase in inhibitory activity compared to compound **2**). Indeed, **6** showed an IC$_{50}$ value of 0.068 μM towards C3 and more than 15-fold selectivity over C2. In comparison to reference ASP9521, compound **6** shows similar potency towards AKR1C3 in the enzymatic assay and similar C3 selectivity over C2 (Table 1). On the other hand, *meta*-phenyl-substituted compound **5** showed less potent AKR1C3 inhibition, with an IC$_{50}$ value of 0.42 μM, and more than 10-fold selectivity for C3 over C2. The unsubstituted phenoxy substituent on the aniline moiety also seemed to be permitted, as it slightly improves activity. Specifically, *meta*-phenoxy-substituted compound **3** showed potent AKR1C3 inhibition, with an IC$_{50}$ value of 0.16 μM and 6-fold selectivity for C3 over C2, whereas *para*-substituted compound **4** displayed an IC$_{50}$ of 0.11 μM and >45-fold selectivity. While these substitutions on the phenoxy ring are detrimental for inhibition activity (compound **4a** and **4b**), substitutions on the phenyl ring, methoxy, hydroxy and trifluoromethyl substitution (**5a-c**, **6b-g**) increased compound activity, except for in compounds **5d** and **6a** (Table 1). In particular, the *ortho*- and *para*-trifluoromethyl substituted derivatives (compounds **6e** and **6g**, respectively) were found to be the most potent AKR1C3 inhibitors of the series (see Table 1).

2.4. Physicochemical characterization: drug-like properties (solubility, ionization, lipophilicity)

The main physicochemical parameters that define the drug-like properties of the compounds were investigated. Solubility at physiological pH was evaluated in phosphate-buffered saline (PBS, pH 7.4) at 25 °C (Table 2). With the exception of phenol-substituted compound **4b**, all of the 3-hydroxybenzoisoxazole derivatives **3–6** showed lower solubility than **2**, and this is due to the presence of an additional phenyl ring. The solubilities of compounds **5, 6, 6a, 6e, 6f** and **6g** was not measurable because lower than the limit of detection (<1 μM) of the UHPLC method used for the quantitative analyses. The low solubility in PBS do not hamper the biological assays, that were conducted in different media and higher temperatures (37 °C). The ionization of the hydroxy function on the benzisoazole ring was evaluated for the most soluble compounds **5b, 5d**, and **6b** which were taken as a reference. The measured pK$_a$ was around 5 (4.96 and 4.99 respectively), meaning that there is a significant amount of compound in the ionized form at physiological pH. Lipophilicity was determined at physiological pH (logD$^{7.4}$) in the PBS/*n*-octanol system. With the exception of compounds **6e-g**, for which lipophilicity values were not determinable due to poor solubility, all of the other compounds showed good lipophilic-hydrophilic balance. As for compound **2**, the measured logD$^{7.4}$ values fell in the 2.4–3.1 range, which is optimal for favorable pharmacokinetic properties. The

Scheme 2. Reagents and conditions: a) thionyl chloride, DMF (catalytic), THF, reflux; b) $NH_2OH \cdot HCl$, K_2CO_3, THF, H_2O, rt. Yield of a + b: 91%; c) 8 M KOH, reflux, then aq. HCl, rt, yield 62%; d) benzylbromide, Ag_2O, DMF, rt, yield of **15a**: 41%; e) Cs_2CO_3, 5 mol% $Pd(OAc)_2$, 8 mol% BINAP, toluene, reflux, yield: 63–78 %; f) TFA, thioanisole, rt, yield 67–80 %; g) 20 mol% $Pd(PPh_3)_4$, K_2CO_3, dioxane/H_2O 9/1 v/v, 90 °C, yield: 23–71 %.

difference between the calculated logP value for the neutral forms (CLOGP) of the compounds and the measured $logD^{7.4}$ value was in agreement with the considerable ionization of the 3-hydroxybenzoisoxazole core at physiological pH. Additionally, ligand-lipophilicity efficiency (LLE) was also calculated (Table 2). LLE is a measure of "drug-likeness" and takes into account the lipophilicity and potency of compounds [42,43]. Most compounds exhibited a more favorable LLE profile than reference **2**.

2.5. Effect of inhibition of AKR1C3 on cell proliferation and PSA expression

All the compounds above described have been characterized for their inhibitor activity towards the purified AKR1C3 enzyme. Next, it was important to investigate the effect of inhibition of AKR1C3 in cell-based environment. For this purpose, 22RV1 cells were chosen as these naturally express AKR1C3 (Fig. 8) and are hormone therapy resistant cells [19], hence can be used to recapitulate CRPC disease.

The effect of the above compounds was evaluated on cell proliferation. Cell viability was assessed using the sulforhodamine B (SRB) assay [30], and the determined IC_{50} values are reported in Table 2. The activity trend presented by the compounds does not fully reflect the IC_{50} values measured for enzyme inhibition and is not even correlated with the lipophilic properties of the compounds, as described by their $logD^{7.4}$. Except for compounds **3**, **5** and **5a-d**, all the other derivatives exhibited a more pronounced antiproliferative effect than reference **2**, which demonstrates how *meta* substitution on the first phenyl ring is detrimental to cellular activity.

The demethylation of **4a**, **5c** and **6a** to obtain hydroxyl derivatives **4b**, **5d** and **6b** improves the solubility of the compounds by about an order of magnitude, although it lowers their $logD^{7.4}$ by 0.1–0.4 units and

is detrimental to cellular activity. The most active compounds against 22RV1 cells are the distal unsubstituted *para*-phenyl derivative **6** (IC_{50} = 8.11 μM), the *meta'*-methoxy-*p*-phenyl derivative **6a** (IC_{50} = 2.34 μM) and the *orto'* and *meta'*-trifluoromethyl-*para*-phenyl derivatives **6e** and **6f** (IC_{50} = 2.013 and 2.39 μM, respectively). Notably, the other substitutions applied to the distal phenyl were detrimental. The distal unsubstituted *para*-phenyl and *para*-phenyloxy derivatives **4** and **6** and **6b** have the most favorable ligand-lipophilicity efficiency of the most active compounds (LLE = 4.16, 4.27 and 4.27, respectively). The distal substituted *para*-phenyl derivative compounds **6a**, **6e** and **6f**, presented the best IC_{50} values in series (2.34, 2.013 and 2.39 μM, respectively) showing that the methoxy group in the meta position (**6a**) and the trifluoromethyl group in ortho (**6e**) and meta (**6f**) positions contribute to cellular potency, although this trend is only partially in line with their enzymatic potency. Surprisingly, *p*-trifluoromethyl substitution gave slightly lower activity, as demonstrated by the IC_{50} value of compound **6g** (19.60 μM), which does not fully reflect the high IC_{50} observed in the enzyme inhibition experiments (0.046 μM). In fact, compound **6g**, which is the most potent enzymatic inhibitor in this series (IC_{50} = 0.046 μM), does not show the best effect in inhibiting 22RV1 cell proliferation.

Two of the most potent AKR1C3 inhibitors (compounds **6** and **6e**) were evaluated for their potential to reduce prostate-specific-antigen (PSA) expression in 22RV1 cells. This experiment evaluated whether the observed cell-growth inhibition is produced by a decrease in the steroidogenic pathway caused by AKR1C3 inhibition. Cells were incubated with the compounds at two different concentrations, one similar to the IC_{50} value of the antiproliferative activity and a ten-fold lower concentration. As this cell line also secretes PSA, PSA levels were measured in cell extracts by Western Blotting, and ß-actin was used as the loading control (Fig. 6). As shown, both compounds were able to reduce the PSA levels at the highest concentration. Compound **6** also
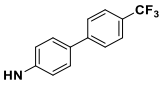
Table 1

Inhibitory activity of compounds **2** – **6g** against AKR1C3 and AKR1C2 recombinant purified enzymes.
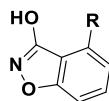
	R =	AKR1C3 IC$_{50}$±SE (µM)	AKR1C2 % Inhibition ±SE at 5 µM (A) or 1 µM (B)[a]
2		0.26 ± 0.03	IC$_{50}$ 118.55 ± 0.03 µm [31]
3		0.16 ± 0.01	90.75 ± 0.83 (A) 49.67 ± 3.01 (B)
4		0.11 ± 0.01	22.86 ± 2.14 (A)
4a		0.51 ± 0.02	29.88 ± 0.82 (A)
4b		0.63 ± 0.03	17.49 ± 1.62 (A)
5		0.42 ± 0.02	47.01 ± 1.51 (A)
5a		0.27 ± 0.01	54.97 ± 1.72 (A)
5b		0.19 ± 0.04	42.05 ± 1.65 (A)
5c		0.19 ± 0.01	51.43 ± 2.80 (A)
5d		0.51 ± 0.02	50.27 ± 3.48 (A)
6		0.068 ± 0.005	11.93 ± 3.87 (B)
6a		0.35 ± 0.01	15.45 ± 1.43 (B)
6b		0.10 ± 0.004	13.61 ± 6.70 (B)
6e		0.060 ± 0.001	13.38 ± 3.41 (B)
6f		0.12 ± 0.003	26.37 ± 3.45 (B)

Table 1 (*continued*)

	R =	AKR1C3 IC$_{50}$±SE (μM)	AKR1C2 % Inhibition ±SE at 5 μM (A) or 1 μM (B)[a]
6g	(structure: biphenyl with CF$_3$ and HN– substituent)	0.046 ± 0.002	n.d.[b]
ASP9521	See Fig. 1	0.044 ± 0.0025	11.29 ± 1.97 (B)

[a]All compounds were tested at 5 μM concentration. The concentration was reduced to 1 μM for compounds emitting strong fluorescence signals at the 460 nm wavelength.

[b]This compound emitted a strong fluorescence signal at 1 μM and its inhibition activity could not be tested.

showed a significant effect at the lowest concentration tested. These results confirm that both compounds inhibit PC-cell proliferation by suppressing androgen biosynthesis via AKR1C3 inhibition.

In addition to evaluating the specificity of the compounds on AKR1C3 inhibition and on PC cell proliferation, MRC-5 cells (normal human fetal lung fibroblasts) were also used to provide an indicator of potential normal tissue toxicity [44,45].

Three compounds with different inhibitory effects on AKR1C3 and on 22RV1 cell proliferation (compounds **4**, **6** and **6f**) were tested for their ability to reduce the proliferation of MRC-5 cells. As shown in Table S1, the three compounds were non-toxic at 50 μM, with a survival rate of almost 100 %. Higher mortality was revealed at 100 μM, but considering that this concentration is 8–40 times higher than the IC$_{50}$ value found in 22RV1 cells, safe and tumor-selective treatment using these compounds can be expected *in vivo*.

To evaluate any possible enhanced effect that may occur when used in combination with currently used drugs, compounds **6** and **6e** were explored with ABI (Fig. 7). A co-treatment with increasing concentrations of the compounds was performed for 72 h. The compound concentrations were chosen to be in the ranges of their specific IC$_{50}$ values. A significant reduction in cell proliferation was observed at all the tested concentrations when cpds **6** and **6e** were added together with ABI. The combination improved the effect observed when ABI is used alone (IC$_{50}$ = 9.09 μM) especially for compound **6e**, which showed an Enhancement Factor (EF) of 2.60. Compound **6** only exhibited an EF of 1.33 (Table S2).

These experiments confirm the potential of the co-administration of CYP171A1-and AKR1C3-targeting compounds to greatly influence key steps in the steroidogenic pathway by reducing PSA production and cell-tumor proliferation [46,47].

2.6. Inhibition of AKR1C3 activity using coumberone assay

AKR1C3 activity was measured in 22RV1, parental LNCaP and LNCaP AKR1C3-transfected sub-lines, using the AKR1C substrate coumberone. The aforementioned compound is metabolized by AKR1C3 into the correspondent fluorescent alcohol (coumberol), which allows enzyme activity to be quantified [48]. Prior to evaluating coumberone metabolism, the expression of AKR1C3 was analyzed using Western blot and, as expected, AKR1C3 expression was only confirmed for the LNCaP (AKR1C3) and 22RV1 cells (Fig. 8a). 10 μM of coumberone was used to achieve a detectable fluorescent output of coumberol, and fluorescence was recorded after 24 h of incubation. At this concentration, coumberol production was found to be approx. 4-fold and 20-fold higher in the 22RV1 and LNCaP-transfected cells, respectively, than in the control LNCaP cells (Fig. 8b).

Three of the most potent AKR1C3 inhibitors **6**, **6g** and **6e** were tested in 22RV1 and LNCaP-AKR1C3 transfected cells to measure their ability to reduce AKR1C3-associated coumberol production. Cells were treated with the three compounds at concentrations similar to their IC$_{50}$ values, which were calculated for the specific cell line using the SRB assay. To measure their impact on AKR1C3 functional activity without significant cell killing, treatment was assessed for only 24 h. In 22RV1 cells, all three compounds reduced coumberol production by around 50 %

(Fig. 9). Similarly, in transfected LNCaP-AKR1C3 cells, all compounds were able to reduce AKR1C3 activity, but in a lower percentage range (20–40 %). It is possible that the artificially high level of enzyme in the AKR1C3-transfected cell line required higher inhibitor concentrations to elicit inhibition at levels similar to those seen in the naturally AKR1C3-expressing cell line.

2.7. Inhibition of AKR1C3 activity using testosterone assay

In order to explore the AKR1C3-targeting compounds' efficacy in reducing testosterone production in the androgen biosynthetic pathway, an Elisa assay was performed using 22RV1 cells. Compounds **6**, **6g** and **6e** were evaluated at two concentrations and an assessment was carried out after 24 h. All of the compounds provided a statistically significant reduction in testosterone production at the highest concentration tested, confirming the existence of a dose-dependent effect (Fig. 10). The highest inhibition was achieved using compound **6**, which was shown to significantly reduce the production of testosterone even when tested at a concentration that was 50-times lower than its IC$_{50}$ value.

2.8. Analysis of the binding affinity of compound **6b** compared to compound **2** and **6**

The most promising candidate for co-crystallization experiments was compound **6b** because of its acceptable solubility in PBS and low IC$_{50}$ (Table 2). To confirm our choice, we compared its binding affinity at equilibrium with that of two other compounds: compound **2** was used as a reference and compound **6** as one of those with the most promising inhibitory properties against the isolated enzyme (Table 1). The results obtained using microscale thermophoresis are described in Table 3 and Fig. S4. In line with the inhibition of AKR1C3 described above, compound **2** has the lowest affinity (K_d = 5.2 μM). Compounds **6b** and **6** were found to bind AKR1C3 with a K_d of 2.5 μM and 3.0 μM, respectively. As the binding affinities were very similar, and as **6b** was more soluble than compound **6** (Table 2), **6b** was chosen as the best candidate for co-crystallization experiments.
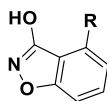
2.9. Analysis of the binding mode of compound **6b** co-crystallized with AKR1C3

The crystal structure of AKR1C3 in a complex with compound **6b** was determined to a resolution of 2.0 Å. X-ray data collection and refinement statistics are summarized in Table S5. The ligand-binding pocket of AKR1C3 is composed of several compartments and compound **6b** was clearly identified in the androstenedione oxyanion binding site (OS) (Fig. 11). However, the electron density map observed for compound **6b** in the binding site of chain B (Fig. S5B) might indicate a partly occupied binding site (approx. 80%). This may be due to the compound low solubility.

The structure of AKR1C3 complexed with compound **6b** reveals that **6b** establishes key interactions with the catalytic residues Tyr55 and His117 from the 3-hydroxybenzoisoxazole moiety (2.7 and 3.0 Å, respectively) (Fig. 11). The compound is also observed to stack with the
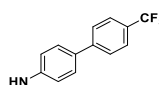
Table 2
Antiproliferative activity (IC$_{50}$) of compounds **2**–**6g** against PC-cell line 22RV1 (SRB assay), solubility (in PBS at pH 7.4), lipophilicity (measured logD$^{7.4}$) and CLOGP. pK$_a$ values were measured for three selected compounds (**5b**, **5d** and **6b**). Ligand-lipophilicity efficiency (LLE) is reported where calculable.

	R =	22RV1 IC$_{50}$±SE (μM)	Solubility PBS (μM)	logD$^{7.4}$±SE [pKa]	CLOGP[e]	LLE[f]
2	3,5-bis(CF$_3$)-phenyl-NH	26.70 ± 1.83	34.1	3.0 ± 0.2	5.84	3.59
3	3-phenoxy-phenyl-NH	58.27 ± 1.68	25.6	3.1 ± 0.2	5.60	3.70
4	4-phenoxy-phenyl-NH	11.81 ± 0.30	13.77	2.8 ± 0.2	5.60	4.16
4a	4-(3-methoxyphenoxy)phenyl-NH	22.43 ± 0.76	5.6	2.79 ± 0.07	5.52	3.50
4b	4-(3-hydroxyphenoxy)phenyl-NH	27.33 ± 0.44	39.7	2.40 ± 0.02	4.93	3.80
5	3-biphenyl-NH	58.20 ± 1.51	<1[d]	2.9 ± 0.2	5.69	3.48
5a	3'-methoxy-biphenyl-3-yl-NH	37.04 ± 0.26	1.8	3.0 ± 0.1	5.61	3.57
5b	3'-hydroxy-biphenyl-3-yl-NH	40.96 ± 0.69	13.7	2.75 ± 0.05 [4.96 ± 0.06 10.6 ± 0.3][a]	5.02	3.97
5c	4'-methoxy-biphenyl-3-yl-NH	31.98 ± 0.36	2.1	2.9 ± 0.2	5.61	3.82
5d	4'-hydroxy-biphenyl-3-yl-NH	56.71 ± 0.85	11.4	2.71 ± 0.05 [4.99 ± 0.05 10.5 ± 0.2][a]	5.02	3.58
6	4-biphenyl-NH	8.11 ± 0.57	<1[d]	2.9 ± 0.3	5.69	4.27
6a	3'-methoxy-biphenyl-4-yl-NH$_2$	2.34 ± 0.06	<1[d]	2.8 ± 0.2	5.61	3.66
6b	3'-hydroxy-biphenyl-4-yl-NH	16.43 ± 0.72	11.1	2.73 ± 0.04 [5.72; 10.44][b]	5.02	4.27
6e	2'-CF$_3$-biphenyl-4-yl-NH	2.013 ± 0.064	<1[d]	n.d.[c]	6.59	–
6f	3'-CF$_3$-biphenyl-4-yl-NH	2.39 ± 0.09	<1[d]	n.d.[c]	6.59	–

(*continued on next page*)

Table 2 (*continued*)

	R =	22RV1 IC$_{50}$±SE (μM)	Solubility PBS (μM)	logD$^{7.4}$±SE [pKa]	CLOGP[e]	LLE[f]
6g	(structure: biphenyl with CF$_3$, HN–)	19.60 ± 0.39	<1[d]	n.d.[c]	6.59	–
ASP9521	See Fig. 1	>50 [34.81% ± 2.95 at 50 μM]	246 μM	2.36 ± 0.05	2.36	5.00

[a] Spectrophotometric determination.
[b] Potentiometric determination (measured by adding 52 % of MDM to the medium, see *Experimental Section*, on a Syrius T3 Instrument by CASSMedChem).
[c] Not determined because of low solubility in the aqueous phase.
[d] Not determined because the value is lower than the limit of detection (LOD = 1 μM) of the UHPLC method.
[e] Calculated using Bio-Loom for Windows, vers. 1.4 (BioByte Corp, Claremont, CA U.S.A).
[f] Calculated as LLE = pIC$_{50}$ – logD$^{7.4}$,according to Murray et al. [42].
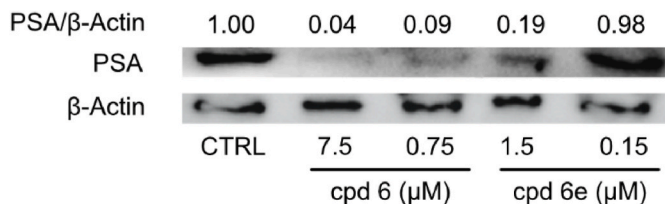

Fig. 6. Inhibition of PSA expression in 22RV1 cells. The Western Blot analysis was performed on cell extracts of 22RV1 cultures incubated for 72 h with compounds **6** and **6e** at two different concentrations. PSA/β-actin values are calculated as fold change. The experiment was performed in duplicate.

benzamide moiety of NADP+ and to form hydrophobic contact with the hydrophobic cavity lined by Tyr24, Trp227 and Phe306, which is part of the steroid channel (SC). The distal 3-hydroxyphenyl moiety establishes hydrogen bonds with the side chain of Ser87 and the backbone carbonyl oxygen of Met120, 2.8 and 2.3 Å, respectively. This moiety is surrounded by the hydrophobic pocket, Trp86, Ser118, Met120 and Phe311, with these residues being part of the SP1 and SP2 compartments. The center aniline moiety is perpendicular to Trp86, and the aniline N–H interacts with the benzamide carbonyl oxygen of NADP+. The electron densities for the side chains of residues Trp227 and Phe306 are very weak, and this might indicate that the side chains are flexible, possibly adopting several conformations.

The binding pose of **6b** observed in the crystal structure is almost identical to that predicted by molecular docking. As expected, the two phenyl rings of the biphenyl moiety assume a twisted conformation similar to the conformation found by molecular docking. This conformation is likely to be essential for establishing optimal interactions with the hydrophobic residues lining the pocket. The dihedral angle of **6b** in the crystal structure is 47° (chain A), while that predicted by docking was 60°, thus supporting the reliability of the *in-silico* predictions.

3. Conclusion

Being an enzyme overexpressed in several radiotherapy- and chemotherapy-resistant cancers types, AKR1C3 is an interesting target that, however, currently has no inhibitor in therapy. In this manuscript, we have described the study of a new series of potent AKR1C3 3-hydroxybenzoisoxazole inhibitors with high selectivity over the AKR1C2 isoforms and micromolar activity in inhibiting 22Rv1 PC-cell proliferation. These compounds act by suppressing androgen biosynthesis via AKR1C3 inhibition as shown by a reduction in PSA levels in cells incubated with new inhibitors and functional activity as measured via reduction of AKR1C3-associated coumberol production. While *in-silico* studies guided the design of the new derivatives, the crystal structures of the AKR1C3 in complex with NADP+ and inhibitor **6b** confirmed the determinants for their potent inhibitory activity. Both *in-silico* studies and crystal structure highlight the importance of allowing 90° rotation around the single bond of the biphenyl group, in ensuring an optimal inhibitor binding mode within the pocket. The *para*-biphenyl that either bears *meta*-methoxy or *ortho*- or *meta*-trifluoromethyl substituents (in compounds **6a**, **6e** and **6f**, respectively) proved to be the best contributors to cellular potency, although this trend was only partially in line with their enzymatic potency. Furthermore, some model compounds (**4**, **6** and **6f**) were tested for their toxicity against human MRC-5 cells, and were found to be
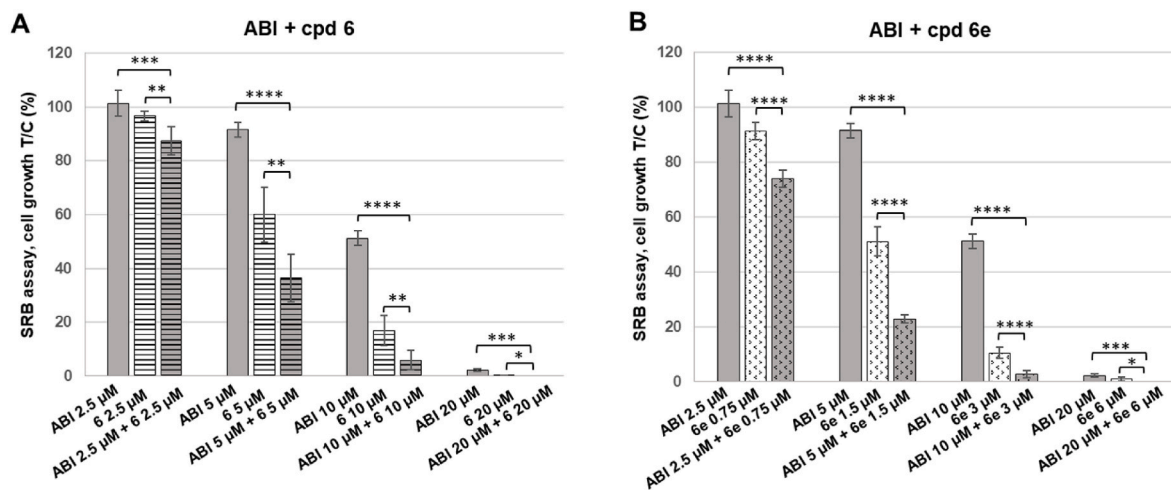

Fig. 7. Cell-proliferation assay performed in 22RV1 cells after 72 h of treatment with escalating concentrations of ABI, compound **6**, compound **6e** and the combination of these compounds. Cell growth is expressed as % T/C (mean OD of treated cells/mean OD of control cells X 100). *P ≤ 0.05, **P ≤ 0.01, ***P ≤ 0.001, ****P ≤ 0.0001.
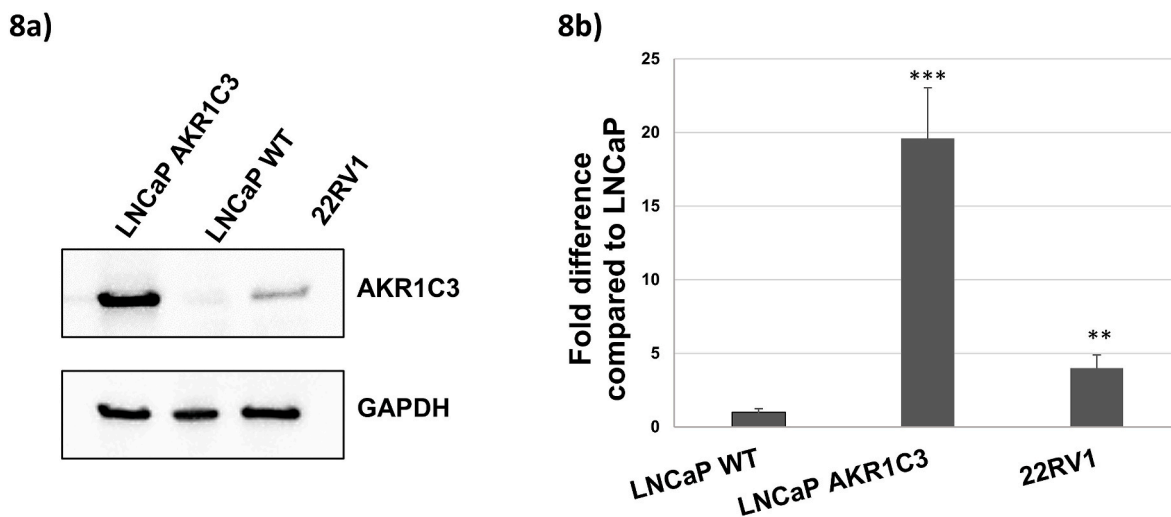
8a)

8b)

Fig. 8. (a) AKR1C3 protein level and (b) coumberone metabolism in different PC cell lines. Coumberol production was reported as fold change compared to LNCaP WT cells. **P ≤ 0.01, ***P ≤ 0.001.

9a) **22RV1**
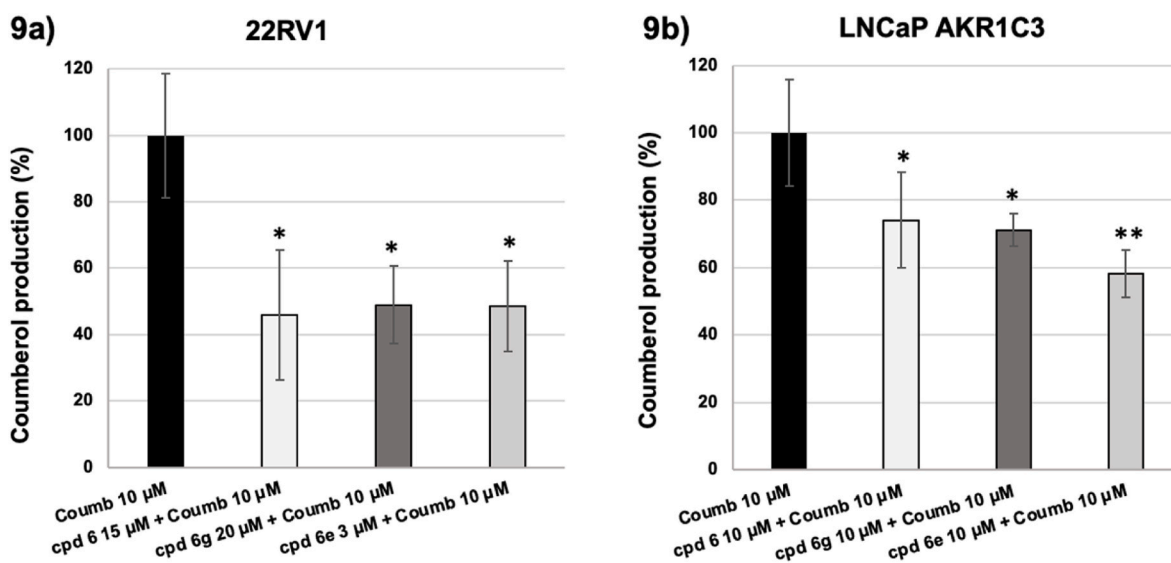

9b) **LNCaP AKR1C3**

Fig. 9. Inhibition of coumberol formation in 22RV1 (9a) and LNCaP (AKR1C3) (9b) cells, after 1 h of pre-treatment with compounds **6**, **6g** and **6e** followed by 24 h of coumberone treatment (10 μM). *P ≤ 0.05, **P ≤ 0.01.
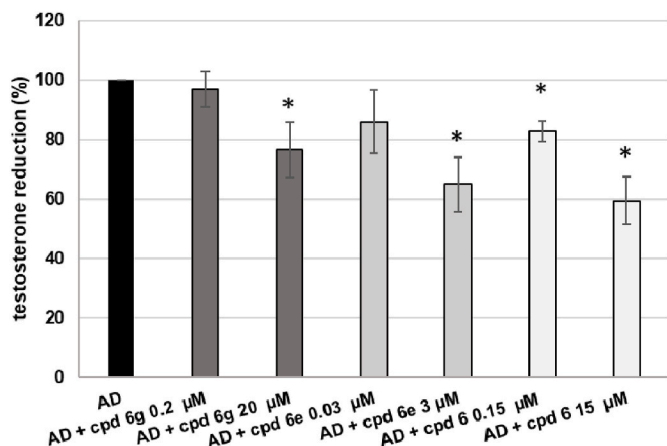

Fig. 10. Inhibition of testosterone production exerted by compounds **6**, **6g** and **6e** in AD-treated 22RV1 cells at two different concentrations. *P ≤ 0.05.

Table 3
Microscale thermophoresis derived K_d values of compounds **2**, **6b** and **6** to the AKR1C3 protein.

AKR1C3 (μM)	Compound	$[L]_0$ (μM)	K_d (μM)
0.005	**2**	150	5.2 ± 0.9
0.005	**6b**	75	2.5 ± 0.4
0.005	**6**	75	3.0 ± 0.5

non-toxic as they do not markedly reduce MRC-5 cell proliferation. Co-treatment with scalar dilutions of either compound **6** or **6e** together with the currently used drug ABI provided a significant reduction in cell proliferation. Specifically, compound **6e** showed an Enhancement Factor (EF) of 2.60, and thus confirmed its potential to intervene in key steps of the steroidogenic pathway with both CYP17A1 and AKR1C3-targeting compounds. The novel compounds reported here possess the features required for promising preclinical/clinical development, as they have been demonstrated to intervene in the steroidogenic pathway and reduce both PSA and testosterone production. Compounds **6a**, **6e**
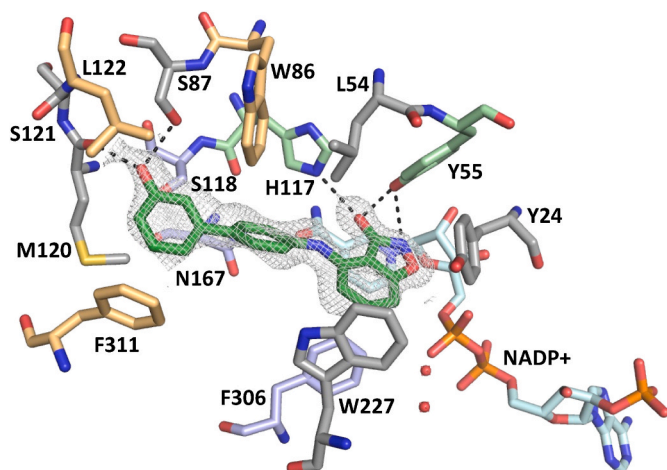
Fig. 11. Crystal structure of compound **6b** in complex with the AKR1C3 binding site of chain A. The ligand and residues lining the pocket within 5 Å of **6b** are shown as sticks, compound **6b** is green and NADP+ is pale cyan. Residues are labeled and colored differently according to the sub-pockets they belong to (pale green: OS; light blue: SP1; light orange: SP2). A simple 2Fo-Fc omit electron density map is shown, displayed at 1σ and carved at 1.8 Å around **6b**. Water molecules are shown as red spheres, hydrogen bonds as black dashed lines.

and **6f**, in particularly, display desirable biochemical potency together with cellular target inhibition and good *in-vitro* ADME properties, which highlight their potential for further development.

4. Experimental section

4.1. Molecular modeling

The X-ray structures of *AKR1C3,* available in the Protein Data Bank (PDB) (https://www.rcsb.org/), were collected and ranked according to resolution, structure integrity and the presence of a co-crystallized ligand. Different X-ray structures were aligned to assess the mobility of specific residues and identify crystallographic water molecules. The crystal structure of AKR1C3 in complex with compound **2** (PDB ID: 6F78) [31] was retrieved from the PDB and properly prepared using the Protein Preparation Wizard tool implemented in Maestro GUI; amendments, such as the addition of hydrogen atoms, assigning bond orders and fixing the charges, were incorporated and the complex then underwent optimization of the hydrogen bond network and restrained minimization. The co-crystallized ligand and cofactor NADP$^+$ were kept as well as three water molecules that were involved in a hydrogen bonding network, while non-structural waters and impurities were removed. The designed candidates, built using 2D sketcher panel in Maestro, were submitted to ligand preparation using the LigPrep module, and their protonation/tautomeric state was checked using MoKa [49]. All simulations took the 3-hydroxybenzoisoxazole moiety as being deprotonated, which is in line with experimental data [29,50,51]. Due to the high flexibility of the binding site, induced-fit docking simulations [52–54], were carried out using the extra-precision (XP) protocol [55], with the OPLS_2005 force field. The grid was centered on the co-crystallized ligand and three residues (Phe306, Phe311, Trp227) were trimmed during the first round of Glide ligand docking (Schrodinger version 2022-4). Residues within 5.0 Å of ligands were refined, except for His117 and Tyr55, which are involved in the stabilization of the negatively charged 3-hydroxybenzoisoxazole core. No constraints were applied throughout the entire procedure. Furthermore, the protocol was validated by re-docking the co-crystallized ligand **2** (Fig. 2b) and flufenamic acid in the protein binding site.

4.2. Chemistry

4.2.1. General methods

All chemical reagents were obtained from commercial sources (Sigma Aldrich, Alfa Aesar, Fluorochem) and used without further purification.

All the components for the buffers, culture media, cell culture supplements, Sulforhodamine B (SRB), isopropyl b- D-1-thiogalactopyranoside (IPTG), DNase, lysozyme, NADP$^+$, S-tetralol were obtained from Sigma-Aldrich (Italy), unless otherwise specified. Analytical-grade solvents (acetonitrile, diisopropyl ether, diethyl ether, dichloromethane [DCM], dimethylformamide [DMF], ethanol 99.8 % v/v, ethyl acetate, methanol [MeOH], petroleum ether b.p. 40–60 °C [petroleum ether]) were used without further purification. When needed, solvents were dried on 4 Å molecular sieves. Tetrahydrofuran (THF) was distilled from Na and benzophenone under N$_2$ immediately prior to use. Thin layer chromatography (TLC) on silica gel was carried out using 5 × 20 cm plates with 0.25 mm layer thickness to monitor the progress of the reactions. Anhydrous Na$_2$SO$_4$ was used as a drying agent for the organic phases. Compound purification was achieved using flash column chromatography on silica gel (Merck Kieselgel 60, 230–400 mesh ASTM) and the indicated eluents. The purity of the final compounds was at least 95%. Purity was checked using two HPLC analytical methods, performed on a UHPLC chromatographic system (Perkin Elmer, Flexar) or HP 1100 chromatograph system (Agilent Technologies, Palo Alto, CA, USA) (see Supplementary). The analytical column for UHPLC system was a UHPLC XBridge BEH C18 XP Column (2.1 × 100 mm, 2.5 μm particle size) (Waters). Compounds were dissolved in methanol and injected through a 20 μl loop. The mobile phase consisted of methanol/water with 0.1 % trifluoroacetic acid. UHPLC analyses were run at flow rates of 0.5 mL/min, and the column effluent was monitored at 230 and 254 nm, referenced against a 500 nm wavelength. The chromatograms of one of the two methods are reported in Supplementary. Melting points (m.p.) were measured on capillary apparatus (Büchi 540) by placing the sample at a temperature 10 °C below the m.p. and applying a heating rate of 2 °C min^{-1}. All compounds were routinely checked using ^{1}H and ^{13}C NMR and mass spectrometry. ^{19}FNMR of new fluorinated compounds are also reported. NMR spectra were performed on a JEOL ECZR600 instrument. The following abbreviations are used for coupling patterns: br = broad, s = singlet, d = doublet, dd = doublet of doublets, t = triplet, q = quartet, quint = quintuplet, m = multiplet. Chemical shifts (δ) are given in parts per million (ppm). The ^{1}H, ^{13}C and ^{19}F NMR spectra of new compounds are shown in the supplementary data. MS spectra were performed on a Waters Micromass ZQ equipped with an ESCi source for electrospray ionization mass spectra (ESI). The HRMS spectra of the final compounds (compounds **3**–**12**) were recorded on a LTQ Orbitrap XL plus (Thermo Fisher Scientific, Waltham, MA USA) equipped with an ESI ionization source with positive and negative ions (Spray capillary voltage: 3000 V (+), 2500 V (−)). Compound **7** was prepared following previously described procedures [31].

4.2.2. General procedure for compounds *10a-c, 11a-e* and *18a-c* (Buchwald-Hartwig reaction)

A suspension of Pd(OAc)$_2$ (0.022 mmol) and (±)-BINAP (0.035 mmol) in dry toluene (15 mL) was allowed to stir at rt for 10 min under a nitrogen atmosphere. Next, bromoaryl derivative **7** or **15a** (0.44 mmol), the appropriate aniline (phenoxyanilines **8a-c** or phenylanilines **9a-e** or **17 a-c** (0.44 mmol)) and Cs$_2$CO$_3$ (0.62 mmol) were added. The reaction mixture was stirred at reflux for 2–4 h, was then cooled to rt and diluted with EtOAc (15 mL). The organic layer was washed with 2 N HCl (25 mL) before the aqueous layer was extracted with EtOAc (2 x 25 mL). The combined organic layers were washed with brine and dried over Na$_2$SO$_4$. The solvents were evaporated under reduced pressure affording the crude product, which was purified using flash chromatography.

4-((3-Phenoxyphenyl)amino)-2-(2,4,6-trimethoxybenzyl)benzo[d]isoxazol-3(2H)-one (**10a**).

Flash chromatography eluent: gradient of petroleum ether/ethyl acetate from 80/20 v/v to 70/30 v/v, yield 78%. White solid, m.p. = 93–94 °C. ^{1}H-NMR (600 MHz, CDCl$_3$) δ 3.81 (3H, s), 3.82 (6H, s), 5.14 (2H, s), 6.13 (2H, s), 6.43 (1H, d, J = 8.2 Hz), 6.69 (1H, dd, J = 8.1, 2.3 Hz), 6.87 (1H, d, J = 8.1 Hz), 6.94 (1H, t, J = 2.2 Hz), 7.00 (1H, dd, J = 8.0 Hz, 2.0 Hz), 7.04 (2H, d, J = 7.6 Hz), 7.11 (1H, t, J = 7.4 Hz), 7.24–7.29 (2H, m), 7.34 (2H, t, J = 7.0 Hz), 8.24 (s, 1H). ^{13}C-NMR (151 MHz, CDCl$_3$) δ 38.5, 55.4, 56.0, 90.5, 99.0, 102.8, 103.2, 104.5, 110.8, 113.2, 115.4, 119.2, 123.6, 129.9, 130.4, 134.5, 142.0, 142.9, 157.0, 158.4, 160.1, 161.1, 161.7, 163.4. MS (ESI): 499 [M+H]$^+$.

*4-((4-phenoxyphenyl)amino)-2-(2,4,6-trimethoxybenzyl)benzo[d]isoxazol-3(2H)-one (**10b**).*

Flash chromatography eluent: DCM/ethyl acetate 95/5 v/v, yield 86 %. White solid, m.p. = 143–145 °C. ^{1}H-NMR (600 MHz, CDCl$_3$) δ 3.85 (3H, s), 3.87 (6H, s), 5.19 (2H, s), 6.18 (2H, s), 6.44 (1H, d, J = 7.9 Hz), 6.75 (1H, d, J = 8.1 Hz), 7.03–7.06 (4H, m), 7.12 (1H, t, J = 7.4 Hz), 7.27–7.31 (3H, m), 7.31–7.41 (2H, m), 8.13 (1H, s). ^{13}C-NMR (151 MHz, CDCl$_3$) δ 38.6, 55.4, 56.0, 90.6, 98.2, 102.4, 103.3, 103.6, 118.5, 120.1, 123.1, 123.5, 129.8, 134.6, 135.8, 144.2, 153.2, 157.7, 160.1, 161.3, 161.7, 163.7. MS (ESI) 499 [M+H]$^+$.

*4-((4-(3-Methoxyphenoxy)phenyl)amino)-2-(2,4,6-trimethoxybenzyl)benzo[d]isoxazol-3(2H)-one (**10c**).*

Flash chromatography eluent: DCM/ethyl acetate 99/1 v/v. Yield 93 %. Yellow solid, m.p. = 147–148 °C. ^{1}H-NMR (600 MHz, CDCl$_3$) δ 3.72 (3H, s), 3.75 (3H, s), 3.77 (6H, s), 5.09 (2H, s), 6.08 (2H, s), 6.34 (1H, d, J = 8.2 Hz), 6.51–6.54 (2H, m), 6.58 (1H, dd, J = 8.3, 2.2 Hz), 6.66 (1H, d, J = 8.1), 6.95–6.97 (2H, m) 7.14–7.20 (4H, m), 8.04 (1H, broad s). ^{13}C-NMR (151 MHz, CDCl$_3$) δ 38.6, 55.5, 55.5, 56.1, 90.6, 98.3, 102.5, 103.3, 103.7, 104.5, 108.8, 110.6, 120.4, 123.5, 130.3, 134.6, 136.0, 144.2, 152.9, 159.1, 160.2, 161.1, 161.3, 161.7, 163.7. MS (ESI): 529 [M+H]$^+$.

*4-([1,1'-Biphenyl]-3-ylamino)-2-(2,4,6-trimethoxybenzyl)benzo[d]isoxazol-3(2H)-one (**11a**).* Flash chromatography eluent: petroleum ether/ethyl acetate 70/30 v/v. Yield 68%. Brown solid, m.p. = 133–135 °C. ^{1}H-NMR (600 MHz, CDCl$_3$) δ 3.82 (3H, s), 3.85 (6H, s), 5.17 (2H, s), 6.15 (2H, s), 6.44 (1H, d, J = 8.2 Hz), 6.92 (1H, d, J = 8.1 Hz), 7.27–7.34 (3H, m), 7.34–7.39 (1H, m), 7.42 (1H, t, J = 7.8 Hz), 7.45 (2H, t, J = 7.7 Hz), 7.52 (1H, t, J = 1.19 Hz), 7.60 (2H, d, J = 7.0 Hz), 8.33 (1H, s). ^{13}C-NMR (151 MHz, CDCl$_3$) δ 38.6, 55.5, 56.1, 90.6, 98.7, 102.8, 103.3, 104.2, 119.8, 119.9, 122.3, 127.3, 127.6, 128.9, 129.9, 134.5, 140.9, 140.9, 142.7, 143.6, 160.2, 161.3, 161.8, 163.7. MS (ESI) 483 [M+H]$^+$.

*4-((3'-Methoxy-[1,1'-biphenyl]-3-yl)amino)-2-(2,4,6-trimethoxybenzyl)benzo[d]isoxazol-3(2H)-one (**11b**).* Flash chromatography eluent: petroleum ether/ethyl acetate 60/40 v/v. Yield 69%. Sticky solid, m.p. = 60–61 °C. ^{1}H-NMR (600 MHz, CDCl$_3$) δ 3.81 (3H, s), 3.83 (6H, s), 3.86 (3H, s), 5.16 (2H, s) 6.14 (2H, s), 6.43 (1H, dd, J = 8.2, 1.5 Hz), 6.90 (2H, d, J = 8.1 Hz), 7.12 (1H, s), 7.17 (1H, d, J = 6.8 Hz), 7.25–7.29 (3H, m), 7.35 (1H, t, J = 8.1, Hz), 7.40 (1H, t, J = 7.8, Hz), 7.50 (1H, d, J = 1.7 Hz), 8.30 (1H, broad s). ^{13}C-NMR (151 MHz, CDCl$_3$) δ 38.6, 55.5, 55.6, 56.1, 90.7, 98.7, 102.8, 103.4, 104.3, 112.9, 113.2, 119.8, 120.0, 120.1, 122.3, 129.8, 129.9, 134.6, 140.9, 142.5, 142.6, 143.6, 160.1, 160.2, 161.3, 161.7, 163.7. MS (ESI) 513 [M+H]$^+$.

*4-((4'-Methoxy-[1,1'-biphenyl]-3-yl)amino)-2-(2,4,6-trimethoxybenzyl)benzo[d]isoxazol-3(2H)-one (**11c**).* Flash chromatography eluent: DCM/ethyl acetate 98/2 v/v. Yield 71 %. White solid, m.p. = 164–165 °C. ^{1}H-NMR (600 MHz, CDCl$_3$) δ 3.83 (3H, s) 3.85 (6H, s), 3.86 (3H, s), 5.17 (2H, s), 6.15 (2H, s), 6.44 (1H, d, J = 8.2 Hz), 6.92 (1H, d, J = 8.1 Hz), 7.00 (2H, d, J = 8.8 Hz), 7.21–7.33 (3H, m), 7.39 (1H, t, J = 7.8 Hz), 7.47 (1H, t, J = 1.9 Hz), 7.54 (2H, d, J = 8.8 Hz), 8.30 (1H, very broad s). ^{13}C-NMR (151 MHz, CDCl$_3$) δ 38.6, 55.5, 55.5, 56.1, 90.6, 98.6, 102.7, 103.3, 104.23, 114.4, 119.4, 119.5, 121.9, 128.3, 129.8, 133.4, 134.6, 140.8, 142.2, 143.6, 159.4, 160.2, 161.3, 161.7, 163.6. MS (ESI) 513 [M+H]$^+$

*4-([1,1'-Biphenyl]-4-ylamino)-2-(2,4,6-trimethoxybenzyl)benzo[d]isoxazol-3(2H)-one (**11d**).* Flash chromatography eluent: DCM/ethyl acetate 95/5 v/v. Yield 79 %. Brown solid, m.p. = 149–151 °C. ^{1}H-NMR

(600 MHz, CDCl$_3$) δ 3.83 (3H, s), 3.85 (6H, s), 5.18 (2H, s), 6.16 (2H, s), 6.46 (1H, d, J = 8.2 Hz), 6.93 (1H, d, J = 8.1 Hz), 7.30 (1H, t, J = 8.2 Hz), 7.33 (1H, t, J = 7.3 Hz), 7.37 (2H, d, J = 8.4 Hz), 7.44 (2H, t, J = 7.6 Hz), 7.57–7.62 (4H, m), 8.31 (1H, very broad s). ^{13}C-NMR (151 MHz, CDCl$_3$) δ 38.8, 55.7, 56.3, 90.8, 99.0, 103.0, 103.5, 104.5, 121.4, 127.1, 127.3, 128.3, 129.1, 134.8, 136.3, 140.0, 140.9, 143.6, 160.4, 161.5, 162.0, 163.8. MS (ESI): 483 [M+H]$^+$.

*4-((3'-Methoxy-[1,1'-biphenyl]-4-yl)amino)-2-(2,4,6-trimethoxybenzyl)benzo[d]isoxazol-3(2H)-one (**11e**).* Flash chromatography eluent: gradient of DCM to DCM/ethyl acetate 80/20 v/v. Yield 53 %. White solid, m.p. = 129–130 °C. ^{1}H NMR (600 MHz, CDCl$_3$) δ 3.83 (3H, s), 3.85 (6H, s), 3.88 (3H, s), 5.17 (2H, s), 6.15 (2H, s), 6.45 (1H, d, J = 8.2 Hz), 6.88 (1H, dd, J = 8.1, 1.8 Hz), 6.93 (1H, d, J = 8.2 Hz), 7.13 (1H, s), 7.15–7.22 (1H, m), 7.29 (1H, t, J = 8.2 Hz), 7.34–7.36 (3H, m), 7.58 (2H, d, J = 8.5 Hz), 8.31 (1H, very broad s). ^{13}C NMR (151 MHz, CDCl$_3$) δ 38.6, 55.4, 55.5, 56.1, 90.6, 98.8, 102.8, 103.3, 104.4, 112.5, 112.6, 119.4, 121.1, 128.1, 129.9, 134.6, 135.9, 139.96, 142.3, 143.3, 160.1, 160.2, 161.3, 161.8, 163.6. MS (ESI): 513 [M+H]$^+$.

4.2.3. General procedure for final compounds 3, 4, 4a, 5a, 5c, 6 and 6a

TFA (2 mL) was added to a mixture of the precursor compound (from series **10** or **11**, 0.600 mmol) and triisopropylsilane (0.136 mL, 0.660 mmol) in dry DCM (10 mL). The mixture was stirred for 1 h at rt under an inert atmosphere before it was diluted with DCM (10 mL) and washed with water (20 mL). The aqueous layer was extracted twice with DCM (2 x 20 mL) before the combined organic layers were washed with brine and dried over Na$_2$SO$_4$. The solvent was evaporated under reduced pressure and the crude product was purified using flash chromatography and recrystallized.

*4-((3-Phenoxyphenyl)amino)benzo[d]isoxazol-3-ol (**3**).* Flash chromatography eluent: DCM/ethyl acetate/TFA 95/5/0.1 v/v/v. Yield 73 %. Greenish solid, m.p. = 138–139 °C (from diisopropyl ether). ^{1}H-NMR (600 MHz, DMSO-d_6) δ 6.59 (1H, d, J = 8.1 Hz), 6.88–6.89 (2H, m), 6.93 (1H, d, J = 7.9 Hz), 7.02–7.06 (3H, m), 7.14 (1H, t, J = 7.4 Hz), 7.29 (1H, t, J = 8.1 Hz), 7.36 (1H, t, J = 8.1 Hz), 7.38–7.41 (2H, m), 8.00 (1H, broad s), 12.57 (very broad s, 1H). ^{13}C-NMR (151 MHz, DMSO-d_6) δ 101.0, 104.0, 107.0, 108.9, 111.6, 113.9, 118.9, 123.6, 130.1, 130.5, 132.6, 139.6, 143.4, 156.5, 157.7, 164.8, 165.5. MS (ESI): 319 [M+H]$^+$. ESI−HRMS (m/z): [M − H]$^-$ calcd for C$_{19}$H$_{14}$N$_2$O$_3$, 317.0932; obsd, 317.0930.

*4-((4-Phenoxyphenyl)amino)benzo[d]isoxazol-3-ol (**4**).* Flash chromatography eluent: DCM/ethyl acetate/TFA 95/5/0.1 v/v/v. Yield 75%. White solid, m.p. = 155–156 °C (from diisopropyl ether). ^{1}H-NMR (600 MHz, DMSO-d_6) δ 6.77 (1H, d, J = 8.0 Hz), 6.80 (1H, d, J = 8.2 Hz), 6.97–7.05 (4H, m), 7.11 (1H, t, J = 7.4 Hz), 7.31–7.35 (3H, m), 7.38 (2H, dd, J = 8.5, 7.5 Hz), 7.79 (1H, broad s), 12.66 (1H, very broad, s). ^{13}C-NMR (151 MHz, DMSO-d_6) δ 99.7, 102.8, 104.9, 117.9, 120.0, 122.6, 123.0, 130.0, 132.8, 136.8, 141.2, 151.6, 157.4, 164.8, 166.0. MS (ESI): 319 [M+H]$^+$. ESI−HRMS (m/z): [M − H]$^-$ calcd for C$_{19}$H$_{14}$N$_2$O$_3$, 317.0932; obsd, 317.0930.

*4-((4-(3-Methoxyphenoxy)phenyl)amino)benzo[d]isoxazol-3-ol (**4a**).* Flash chromatography eluent: petroleum ether/ethyl acetate/TFA 80/20/0.1 v/v/v. Yield 56 %. Greenish solid, m.p. = 144–145 °C (from acetonitrile). ^{1}H-NMR (600 MHz, DMSO-d_6) δ 3.73 (3H, s), 6.53 (1H, dd, J = 8.1, 2.0 Hz) 6.56 (1H, t, J = 2.3 Hz), 6.68 (1H, dd, J = 8.3, 2.2 Hz), 6.77 (1H, d, J = 7.8 Hz), 6.80 (1H, d, J = 8.2 Hz), 7.02 (2H, d, J = 8.7 Hz), 7.26 (1H, t, J = 8.2 Hz), 7.29–7.37 (3H, m), 7.78 (1H, broad s), 12.60 (1H, very broad s). [3]C-NMR (151 MHz, DMSO-d_6) δ 55.8, 100.3, 103.3, 104.5, 105.5, 109.1, 110.3, 120.7, 123.0, 131.0, 133.5, 137.4, 141.7, 151.8, 159.2, 161.2, 165.3, 166.3. MS (ESI): 349 [M+H]$^+$. ESI−HRMS (m/z): [M − H]$^-$ calcd for C$_{20}$H$_{16}$N$_2$O$_4$, 347.1037; obsd, 347.1037.

*4-([1,1'-Biphenyl]-3-ylamino)benzo[d]isoxazol-3-ol (**5**).* Flash chromatography eluent: petroleum ether/ethyl acetate/TFA 70/30/0.1 v/v/v. Yield 74 %. White solid, m.p. = 200–203 °C (from DCM). ^{1}H-NMR (600 MHz, DMSO-d_6) δ 6.87 (1H, d, J = 8.2 Hz), 6.96 (1H, d, J = 7.9 Hz),

7.29–7.31 (2H, m), 7.36–7.43 (3H, m), 7.47 (2H, t, J = 7.7 Hz), 7.56 (1H, t, J = 1.9 Hz), 7.66 (2H, d, J = 7.1 Hz), 7.95 (1H, broad s), 12.70 (1H, very broad, s). ^{13}C-NMR (151 MHz, DMSO-d_6) δ 100.5, 103.4, 105.9, 118.1, 118.7, 120.7, 126.7, 127.6, 129.0, 129,8, 130.0, 140.2, 141.4, 141.8, 141.9, 164.8, 165.7. MS (ESI): 303 [M+H]$^+$. ESI−HRMS (m/z): [M − H]$^-$ calcd for $C_{19}H_{14}N_2O_2$, 301.0983; obsd, 301.0982.

4-((3′-Methoxy-[1,1′-biphenyl]-3-yl)amino)benzo[d]isoxazol-3-ol (5a). Flash chromatography eluent: DCM/ethyl acetate 95/5 v/v. Yield 58 %. Pale yellow solid, m.p. = 159–160 °C (from diisopropyl ether). ^{1}H-NMR (600 MHz, DMSO-d_6) δ 3.81 (3H, s), 6.86 (1H, d, J = 8.2 Hz), 6.92–6.95 (2H, m), 7.17 (1H, s), 7.21 (1H, d, J = 7.8 Hz), 7.28–7.31 (2H, m), 7.33–7.45 (3H, m), 7.55 (1H, s), 7.93 (1H, broad s). ^{13}C-NMR (151 MHz, DMSO-d_6) δ 55.2, 100.4, 103.4, 106.0, 112.2, 113.2, 118.3, 118.8, 119.1, 120.8, 129.8, 130.0, 132.9, 140.3, 141.3, 141.7, 141.8, 159.8, 164.8, 165.8. MS (ESI): 333 [M+H]$^+$. ESI−HRMS (m/z): [M − H]$^-$ calcd for $C_{20}H_{16}N_2O_3$, 331.1088; obsd, 331,1089.

4-((4′-Methoxy-[1,1′-biphenyl]-3-yl)amino)benzo[d]isoxazol-3-ol (5c). Flash chromatography eluent: DCM/ethyl acetate 95/5 v/v. Yield 80%. Pale yellow solid, m.p. = 162–163 °C (from diisopropyl ether). ^{1}H-NMR (600 MHz, DMSO-d_6) δ 3.79 (3H, s), 6.85 (1H, d, J = 8.2 Hz), 6.94 (1H, d, J = 7.9 Hz), 6.99–7.07 (2H, m), 7.21–7.28 (2H, m), 7.38 (2H, td, J = 7.9, 3.3 Hz), 7.50 (1H, s), 7.56–7.64 (2H, m), 7.91 (1H, broad s). ^{13}C-NMR (151 MHz, DMSO-d_6) δ 55.2, 100.3, 103.4, 105.8, 114.4, 117.7, 118.1, 120.3, 127.8, 129.8, 132.4, 133.4, 141.1, 141.7, 159.0, 164.8, 165.9. MS (ESI): 333 [M+H]$^+$. ESI−HRMS (m/z): [M − H]$^-$ calcd for $C_{20}H_{16}N_2O_3$, 331.1088; obsd, 331.1089.

4-([1,1′-Biphenyl]-4-ylamino)benzo[d]isoxazol-3-ol (6). Flash chromatography eluent: DCM/ethyl acetate 95/5 v/v. Yield 37 %. White solid, m.p. = 224–226 °C (from DCM/MeOH 1:1 v/v). ^{1}H-NMR (600 MHz, DMSO-d_6) δ 6.88 (1H, d, J = 8.2 Hz), 6.97 (1H, d, J = 7.9 Hz), 7.32 (1H, t, J = 7.3 Hz), 7.39 (3H, m), 7.43 (2H, t, J = 7.6 Hz), 7.63 (2H, d, J = 8.4 Hz), 7.65 (2H, d, J = 7.6 Hz), 7.98 (1H, broad s), 12.70 (1H, very broad s). ^{13}C-NMR (151 MHz, DMSO-d_6) δ 100.6, 103.6, 106.3, 119.8, 126.1, 126.9, 127.5, 128.9, 132.7, 133.7, 139.8, 140.0, 140.9, 164.8, 165.7. MS (ESI): 303 [M+H]$^+$. ESI−HRMS (m/z): [M − H]$^-$ calcd for $C_{19}H_{14}N_2O_2$, 301.0983; obsd, 301.0985.

4-((3′-Methoxy-[1,1′-biphenyl]-4-yl)amino)benzo[d]isoxazol-3-ol (6a). Flash chromatography eluent: DCM/ethyl acetate 95/5 v/v. Yield 65 %. Greenish solid, m.p. = 181–182 °C (from MeOH). ^{1}H-NMR (600 MHz, DMSO-d_6) δ 3.82 (3H, s), 6.86–6.92 (2H, m), 6.97 (1H, d, J = 7.9 Hz), 7.17 (1H, t, J = 2.1), 7.22 (1H, d, J = 7.7 Hz), 7.33–7.43 (4H, m), 7.65 (2H, d, J = 8.6 Hz), 7.98 (1H, broad s), 12.67 (1H, very broad s). ^{13}C-NMR (151 MHz, DMSO-d_6) δ 55.2, 100.7, 103.7, 106.3, 111.7, 112.6, 118.6, 119.8, 127.7, 130.1, 132.9, 133.7, 140.1, 141.0, 141.4, 159.9, 164.9, 165.9. MS (ESI): 333 [M+H]$^+$. ESI−HRMS (m/z): [M − H]$^-$ calcd for $C_{20}H_{16}N_2O_3$, 331.1088; obsd, 331.1089.

4.2.4. General procedure for final compounds 4b, 5b, 5d and 6b

1 M BBr$_3$ in DCM (1 mL, 1.02 mmol) was diluted in 10 mL of DCM under an inert atmosphere and the resulting solution was cooled to 0 °C. A solution of protected compound (**4a**, **5a**, **5c** or **6a**, 0.085 g, 0.250 mmol) in DCM was slowly added. The reaction mixture was stirred for 5 h at 0 °C before it was quenched using 10 mL water. The two phases were separated and the aqueous phase was extracted with EtOAc (2x20 mL). The organic phases were separately washed with brine and dried over Na$_2$SO$_4$. They were then combined and the solvents were evaporated under reduced pressure. The resulting crude product was purified using flash chromatography and recrystallized with the indicated solvent.

4-((4-(3-Hydroxyphenoxy)phenyl)amino)benzo[d]isoxazol-3-ol (4b). Obtained from **4a**. Flash chromatography eluent: DCM/MeOH/TFA 98/2/0.1 v/v/v. Yield 80 %. Pale yellow solid, m.p. = 196–197 °C (from diisopropyl ether). ^{1}H-NMR (600 MHz, DMSO-d_6) δ 6.36 (1H, t, J = 2.2 Hz), 6.42 (1H, dd, J = 8.1, 1.7 Hz), 6.50 (1H, dd, J = 8.2, 1.6 Hz), 6.77 (1H, d, J = 8.0 Hz), 6.80 (1H, d, J = 8.2 Hz), 7.01 (2H, d, J = 8.8 Hz), 7.14 (1H, t, J = 8.1 Hz), 7.29–7.40 (3H, m, 20), 7.77 (1H, broad s), 9.55 (1H, broad s), 12.64 (1H, very broad s). ^{13}C-NMR (151 MHz, DMSO-d_6)

δ 99.4, 101.2, 102.5, 104.5, 104.6, 108.1, 109.8, 120.0, 122.2, 130.1, 132.6, 136.5, 151.1, 151.4, 158.4, 158.5, 164.5. MS (ESI): 335 [M+H]$^+$. ESI−HRMS (m/z): [M − H]$^-$ calcd for $C_{19}H_{14}N_2O_4$, 333.0881; obsd 333.0881.

4-((3′-Hydroxy-[1,1′-biphenyl]-3-yl)amino)benzo[d]isoxazol-3-ol (5b). Obtained from **5a**. Flash chromatography eluent: DCM/MeOH/TFA 98/2/0.1 v/v/v. Yield 67 %. Gray solid, m.p. = 220–223 °C, dec. (from DCM). ^{1}H-NMR (600 MHz, DMSO-d_6) δ 6.77 (1H, d, J = 7.7 Hz), 6.87 (1H, d, J = 7.9 Hz), 6.95 (1H, d, J = 7.9 Hz), 7.01 (1H, s), 7.06 (1H, d, J = 7.5 Hz), 7.22–7.29 (3H, m), 7.37–7.40 (2H, m), 7.49 (1H, s), 7.95 (1H, broad s), 9.52 (1H, broad s), 12.61 (1H, very broad s). ^{13}C-NMR (151 MHz, DMSO-d_6) δ 100.4, 103.5, 106.0, 113.5, 114.6, 117.4, 117.9, 118.6, 120.5, 129.8, 129.9, 132.8, 140.2, 141.5, 141.9, 141.7, 157.8, 164.8, 166.8. MS (ESI): 319.02 [M+H]$^+$. ESI−HRMS (m/z): [M − H]$^-$ calcd for $C_{19}H_{14}N_2O_3$, 317.0932; obsd 317.0932.

4-((4′-Hydroxy-[1,1′-biphenyl]-3-yl)amino)benzo[d]isoxazol-3-ol (5d). Obtained from **5c**. Flash chromatography eluent: DCM/MeOH 99/1 v/v. Yield 77%. Gray solid, m.p. = 217–218 °C dec. (from diisopropyl ether). ^{1}H-NMR (600 MHz, DMSO-d_6) δ 6.83–6.85 (m, 3H), 6.94 (d, J = 7.9 Hz, 1H), 7.20–7.22 (m, 2H), 7.34–7.39 (m, 2H), 7.46–7.49 (m, 3H), 7.88 (broad s, 1H), 9.55 (broad s, 1H), 12.66 (very broad s, 1H). ^{13}C-NMR (151 MHz, DMSO-d_6) δ 100.2, 103.3, 105.7116.0, 117.6, 117.8, 120.1, 127.8, 129.7, 130.8, 132.9, 141.4, 141.5, 141.6, 157.2, 164.7, 166.7. ESI−HRMS (m/z): [M − H]$^-$ calcd for $C_{19}H_{14}N_2O_3$, 317.0932; obsd 317.0933.

4-((3′-Hydroxy-[1,1′-biphenyl]-4-yl)amino)benzo[d]isoxazol-3-ol (6b). Obtained from **6a**. Flash chromatography eluent: DCM/MeOH/TFA 98/2/0.1 v/v/v. Yield 70 %. Light yellow solid, m.p. = 227–230 °C. ^{1}H-NMR (600 MHz, DMSO-d_6) δ 66.72 (1H, d, J = 8.0 Hz), 6.87 (1H, d, J = 8.2 Hz), 6.95 (1H, d, J = 7.9 Hz), 7.00 (1H, s), 7.05 (1H, d, J = 7.8 Hz), 7.23 (1H, t, J = 7.8 Hz), 7.35 (2H, d, J = 8.5 Hz), 7.38 (1H, t, J = 8.1 Hz), 7.56 (2H, d, J = 8.5 Hz), 7.98 (1H, broad s), 9.52 (1H, very broad s). ^{13}C-NMR (151 MHz, DMSO-d_6) δ 100.5, 103.8, 106.2, 112.9, 113.9, 114.1, 117.0, 119.8, 127.4, 129.9, 133.9, 140.8, 141.3, 149.2, 157.8, 164.8, 165.9. MS (ESI): 341.4 [M+Na]$^+$. ESI−HRMS (m/z): [M − H]$^-$ calcd for $C_{19}H_{14}N_2O_3$, 317.0932; obsd 317.0932.

2-Bromo-6-fluoro-N-hydroxybenzamide (13). Thionyl chloride (1.32 mL, 18.2 mmol) was added dropwise at rt to a solution of 2-bromo-6-fluorobenzoic acid **12** (2.00 g, 9.13 mmol) in dry THF (30 mL) then dry DMF (0.20 mL) was added to the reaction medium. The mixture was heated at reflux for 3 h, then cooled to rt and the solvent, as well as residual thionyl chloride and DMF, were evaporated under reduced pressure. The resulting acyl chloride was dissolved in dry THF (20 mL) and used without any further purification in the next step. Hydroxylammonium chloride (1.90 g, 27.4 mmol) was added to a solution of K$_2$CO$_3$ (6.32 g, 45,7 mmol) in H$_2$O (25 mL) and allowed to stir at rt for 10 min. The acyl chloride solution in THF was added to the aqueous solution of hydroxylamine at 0 °C, observing the formation of a white precipitate. The reaction medium was stirred overnight at rt, then THF was removed at reduced pressure and the concentrated mixture was acidified with 2 M HCl to pH 3. The resulting aqueous phase was extracted with EtOAc (4 x 30 mL) and the combined organic layers were washed with brine and dried over Na$_2$SO$_4$, and then concentrated under vacuum to give **13**. Yield 91 %. Pale yellow solid, m.p. = 161–162 °C. ^{1}H-NMR (600 MHz, DMSO-d_6) δ: 7.33 (1H, t, J = 8.6 Hz), 7.42 (1H, td, J = 8.2, 6.2 Hz), 7.51 (1H, d, J = 8.0 Hz), 9.41 (1H, d, J = 1.5 Hz), 11.12 (1H, s). ^{13}C-NMR (151 MHz, DMSO-d_6) δ 115.6 (d, J = 21.8 Hz), 121.4 (d, J = 4.5 Hz), 126.3 (d, J = 23.0 Hz), 129.1 (d, J = 2.4 Hz), 132.8 (d, J = 8.7 Hz), 159.6 (d, J = 249.6 Hz). ^{19}F NMR (565 MHz, DMSO-d_6) δ: 112.3 (s). MS (ESI) 233 [M+H]$^+$.

4-Bromobenzo[d]isoxazole-3-ol (14). A solution of N-hydroxy-benzamide **13** (1.486 g, 6.35 mmol) in 8 M KOH (2.24 g KOH in 5 mL H$_2$O) was refluxed for 40 h. The resulting red solution was cooled to rt observing the formation of a white precipitate. The precipitate was dissolved by diluting the mixture with in H$_2$O, in the following the medium was acidified with 6 M HCl to pH 2. The resulting suspension

was diluted with water, extracted with EtOAc (3 x 30 mL) and the combined organic layers were washed with brine and dried over Na$_2$SO$_4$ before being removed under vacuum. The reddish solid crude product was recrystallized from acetonitrile to give pure **14**. Yield 62 %. Orange crystals, m.p. = 228–230 °C (from acetonitrile). ^{1}H-NMR (600 MHz, MeO*D*) δ: 7.42–7.45 (3H, m). ^{13}C-NMR (151 MHz, MeO*D*) δ 110.4, 115.3, 115.8, 128.1, 133.0, 165.9, 166.3. MS (ESI) 214 [M + H]$^+$.

3-(Benzyloxy)-4-bromobenzo[d]isoxazole (15a) and *2-benzyl-4-bromobenzo[d]isoxazol-3(2H)-one (15b)*. Ag$_2$O (1.38 g, 5.94 mmol) was added to the solution of **14** (0.848 g, 3.96 mmol) in 5 mL of DMF under a nitrogen atmosphere. The resulting mixture, shielded from light, was stirred for 10 min and then benzylbromide (1.02 g, 5.94 mmol) was added stirring in the following the reaction medium overnight at rt. The crude product was purified by flash column chromatography (petroleum ether/EtOAc from 9/1 to 8/2) to afford the compounds **15a** and **15b**:

15a, yield 41 %, white solid, m.p. = 72–73 °C. ^{1}H-NMR (600 MHz, CDCl$_3$) δ 5.52 (s, 2H), 7.44–7.36 (m, 6H), 7.56 (d, J = 7.5 Hz, 2H). ^{13}C-NMR (151 MHz, CDCl$_3$) δ 71.95, 109.48, 114.31, 114.49, 127.15, 127.67, 128.42, 128.67, 131.48, 135.67, 164.85, 165.79. MS (ESI) 304 [M+H]$^+$.

15b, yield 8 %, white solid, m.p. = 124.5–125 °C. ^{1}H-NMR (600 MHz, CDCl$_3$) δ 5.17 (s, 2H), 7.11 (dd, J = 5.4, 3.7 Hz, 1H), 7.40–7.29 (m, 7H). ^{13}C-NMR (151 MHz, CDCl$_3$) δ 49.8, 109.2, 115.3, 118.7, 127.1, 127.8, 128.4, 128.9, 134.1, 134.6, 161.0, 161.0. MS (ESI) 304 [M+H]$^+$.

4.2.5. General procedure for the preparation of anilines 17 a-c

A solution of 4-bromoaniline (1.0 equiv.), Pd(PPh$_3$)$_4$ (0.2 equiv.) and K$_2$CO$_3$ (4.0 equiv.) in dioxane/H$_2$O (9/1) was stirred for 30 min under a nitrogen atmosphere. The corresponding boronic acid **16 a-c** (3.0 equiv.) was then added in several portions and the reaction medium was heated at 90 °C for 3–4.5 h. After cooling to rt, the reaction was quenched with water (60 mL) and the aqueous phase was extracted with EtOAc. The combined organic layers were washed with saturated brine, dried over Na$_2$SO$_4$ and concentrated under vacuum. The crude product was purified by flash column chromatography.

2'-(Trifluoromethyl)-[1,1'-biphenyl]-4-amine (17a). Flash column chromatography eluent: petroleum ether/EtOAc (100/0 v/v to 80/20 v/v). The product was obtained as a yellow oil in 27 % yield. ^{1}H NMR (600 MHz, CDCl3) δ 3.73 (very broad s, 2H), 6.72 (d, J = 8.4 Hz, 2H), 7.13 (d, J = 8.2 Hz, 2H), 7.33 (d, J = 7.6 Hz, 1H), 7.41 (t, J = 7.7 Hz, 1H), 7.53 (t, J = 7.4 Hz, 1H), 7.72 (d, J = 7.9 Hz, 1H). ^{13}C NMR (151 MHz, CDCl3) δ 114.5, 124.4 (q, J = 273.5 Hz), 126.2 (q, J = 5.4 Hz), 126.9, 129.4, 130.1, 130.3, 131.4, 132.5, 141.8, 146.0. MS (ESI) 238 [M+H]+.

3'-(Trifluoromethyl)-[1,1'-biphenyl]-4-amine (17b). Flash column chromatography eluent: petroleum ether/EtOAc 7/3 v/v. Light yellow solid, m.p. = 65–67 °C. Yield 71 %. ^{1}H NMR (600 MHz, CDCl3) δ: 3.79 (broad s, 2H), 6.78 (d, J = 8.5 Hz, 2H), 7.43 (d, J = 8.5 Hz, 2H), 7.53–7.49 (m, 2H), 7.71 (d, J = 7.0 Hz, 1H), 7.78 (s, 1H). ^{13}C NMR (151 MHz, CDCl3) δ 115.5, 122.9, 123.1, 122.9 (q, J3 = 3.6 Hz), 123.1 (q, J3 = 3.7 Hz), 124.4 (q, J1 = 272.6 Hz), 128.2, 129.2, 129.6, 130.0, 131.1 (q, J2 = 31.9 Hz), 142.0, 146.6. MS (ESI) 238 [M+H]+.

4'-(Trifluoromethyl)-[1,1'-biphenyl]-4-amine (17c). Flash column chromatography eluent: petroleum ether/EtOAc: 8/2 v/v to 7/3 v/v. Yellow solid, m.p. = 141–142 °C. Yield 23 %. ^{1}H-NMR (600 MHz, CDCl$_3$) δ 3.81 (br s, 2H), 6.78 (d, J = 8.5 Hz, 2H), 7.43 (d, J = 8.5 Hz, 2H), 7.58–7.74 (m, 4H). ^{13}C-NMR (151 MHz, CDCl$_3$) δ 115.5, 124.5 (q, J = 271.8 Hz), 125.7, 125.7, 126.5, 128.3, 129.9, 144.7, 146.8. MS (ESI) 238 [M+H]$^+$.

3-(Benzyloxy)-N-(2'-(trifluoromethyl)-[1,1'-biphenyl]-4-yl)benzo[d]isoxazol-4-amine (18a). The Buchwald-Hartwig procedure was performed on 0.238 g (0.78 mmol) of **15a** and *o*-trifluoromethyl-phenyl-4-aniline **17a** (0.186 g, 0.78 mmol). The reaction medium was heated for 1.5 h. Flash column chromatography eluent: petroleum ether/EtOAc 95/5 v/v. White solid, m.p. = 91–93 °C. Yield 64 %. ^{1}H-NMR (600 MHz, CDCl3) δ 5.52 (s, 2H), 6.86 (d, J = 8.3 Hz, 1H), 6.89 (s, 1H), 6.99 (d, J = 7.9 Hz, 1H), 7.23–7.26 (m, 2H), 7.31 (d, J = 8.4 Hz, 2H), 7.33–7.36 (m,

2H), 7.39–7.49 (m, 4H), 7.53–7.59 (m, 3H), 7.76 (d, J = 7.8 Hz, 1H). ^{13}C-NMR (151 MHz, CDCl$_3$ δ 72.7, 100.8, 102.7, 105.0, 120.0, 124.3 (q, J = 273.9 Hz), 126.3 (q, J = 5.3 Hz), 127.4, 128.6, 128.6, 129.0, 129.0, 130.2, 131.5, 132.3, 132.5, 134.9, 135.5, 139.8, 140.2, 141.0, 166.0, 166.6. ^{19}F NMR (565 MHz, DMSO-d_6) δ: 56.7. MS (ESI) 461 [M+H]$^+$.

3-(Benzyloxy)-N-(3'-(trifluoromethyl)-[1,1'-biphenyl]-4-yl)benzo[d]isoxazol-4-amine (18b). The Buchwald-Hartwig procedure was performed on 0.217 g (0.71 mmol) of **15a** and *m*-trifluoromethyl-phenyl-4-aniline **17b** (0.169 g, 0.71 mmol). The reaction medium was heated for 3.5 h. Flash column chromatography eluent: petroleum ether/EtOAc 90/10 v/v. White solid, m.p. = 125–127 °C. Yield 78 %. ^{1}H-NMR (600 MHz, CDCl$_3$) δ 5.52 (s, 2H), 6.88 (d, J = 8.3 Hz, 1H), 6.90 (s, 1H), 6.99 (d, J = 7.9 Hz, 1H), 7.30 (d, J = 8.5 Hz, 2H), 7.35 (t, J = 8.1 Hz, 1H), 7.46–7.40 (m, 2H), 7.59–7.53 (m, 5H), 7.75 (d, J = 7.6 Hz, 1H), 7.82 (s, 1H). ^{13}C-NMR (151 MHz, CDCl$_3$) δ 72.6, 101.0, 102.8, 105.1, 120.8, 123.5 (q, J = 3.9 Hz), 123.7 (q, J = 3.6 Hz), 124.3 (d, J = 272.7 Hz), 128.3, 128.5, 128.9, 129.0, 129.4, 130.0, 131.3 (q, J = 32.1 Hz), 132.4, 134.5, 135.4, 139.5, 140.7, 141.3, 165.9, 166.5. ^{19}F NMR (565 MHz, DMSO-d_6) δ: 62.5. MS (ESI) 461 [M+H]$^+$.

3-(Benzyloxy)-N-(4'-(trifluoromethyl)-[1,1'-biphenyl]-4-yl)benzo[d]isoxazol-4-amine (18c). The Buchwald-Hartwig procedure was performed on 0.221 g (0.73 mmol) of **15a** and *p*-trifluoromethyl-phenyl-4-aniline **17c** (0.172 g, 0.73 mmol). The reaction medium was heated for 1.5 h. Flash column chromatography eluent: petroleum ether/EtOAc 90/10 v/v. White solid, m.p. = 164–165 °C. Yield 63 %. ^{1}H-NMR (600 MHz, CDCl$_3$) δ 5.52 (s, 2H), 6.88 (d, J = 8.28 Hz, 1H), 6.91 (br s, 1H), 7.00 (d, J = 7.92 Hz, 1H), 7.29–7.31 (m, 2H), 7.35 (t, J = 8.13 Hz, 1H), 7.34–7.46 (m, 3H), 7.53 (d, J = 7.2, 2H), 7.57–7.60 (m, 2H), 7.67–7.70 (m, 4H). ^{13}C-NMR (151 MHz, CDCl$_3$) δ 72.7, 101.1, 102.9, 105.3, 120.7, 124.5 (q, J = 271.8 Hz), 125.9 (q, J = 3.8 Hz), 127.0, 128.4, 128.5, 129.0, 129.0, 129.1 (q, J = 33.2 Hz), 132.5, 134.4, 135.5, 139.4, 140.9, 144.1, 166.0, 166.5. ^{19}F NMR (565 MHz, DMSO-d_6) δ: 60.6. MS (ESI) 461 [M+H]$^+$.

4.2.6. General procedure for final compounds 6e, 6f and 6g

3-(Benzyloxy)benzo[d]isoxazole **18 a-c** (1 equiv.) was dissolved in a solution of TFA (volume mL) and thioanisole (6 equiv.), as previously described in the supplementary [56] for similar hydroxy-heterocyclic systems. The reaction mixture was stirred at rt for 20–45 min, then the reaction was quenched by the addition of water (40 mL); the aqueous phase was extracted with EtOAc (3 x 30 mL). The combined organic layers were washed with saturated brine, dried over Na$_2$SO$_4$ and concentrated. The crude product was purified by flash column chromatography and crystallization.

4-((2'-(Trifluoromethyl)-[1,1'-biphenyl]-4-yl)amino)benzo[d]isoxazol-3-ol (6e). Flash column chromatography eluent: gradient from DCM/MeOH 100/0 v/v to 95/5 v/v. White solid, m.p. = 202–203 °C dec (from diisopropyl ether). Yield 67 %. ^{1}H-NMR (600 MHz, DMSO-d_6) δ 6.89 (d, J = 8.2 Hz, 1H), 6.99 (d, J = 7.9 Hz, 1H), 7.26 (d, J = 8.4 Hz, 2H), 7.35 (d, J = 8.5 Hz, 2H), 7.40–7.43 (m, 2H), 7.58 (t, J = 7.7 Hz, 1H), 7.71 (t, J = 7.5 Hz, 1H), 7.82 (d, J = 7.8 Hz, 1H), 7.99 (br s, 1H), 12.62 (very br s, 1H). ^{13}C-NMR (151 MHz, DMSO-d_6) δ 100.7, 103.7, 106.4, 118.6, 124.3 (q, J = 274.0 Hz), 126.1 (q, J = 5.3 Hz), 127.0 (q, J = 29.0 Hz), 127.7, 129.3, 129.6 (q, J = 1.1 Hz), 132.3, 132.3, 132.7, 136.3, 140.6, 141.1, 164.8, 165.6. ^{19}F NMR (565 MHz, DMSO-d_6) δ: 55.2. ESI−HRMS (*m/z*): [M − H]$^-$ calcd for $C_{20}H_{13}F_3N_2O_2$, 369.0856; obsd 369.0855.

4-((3'-(Trifluoromethyl)-[1,1'-biphenyl]-4-yl)amino)benzo[d]isoxazol-3-ol (6f). Flash column chromatography eluent: gradient from DCM/MeOH 100/0 v/v to 95/5 v/v. Light green solid, m.p. = 208–209 °C dec (from diisopropyl ether). Yield 68 %. ^{1}H-NMR (600 MHz, DMSO- d_6) δ 6.92 (d, J = 8.2, 1H), 7.00 (d, J = 7.9 Hz, 1H), 7.39–7.43 (m, 3H), 7.65–7.69 (m, 2H), 7.72 (d, J = 8.5 Hz, 2H), 7.94 (s, 1H), 7.97 (d, J = 6.2 Hz, 1H), 8.07 (br s, 1H). ^{13}C-NMR (151 MHz, DMSO-d_6) δ 100.9, 103.9, 106.9, 119.4, 122.3, 123.3, 124.3 (q, J = 272.4 Hz), 127.8, 129.8 (q, J = 31.6 Hz), 130.0, 130.1, 131.6, 132.7, 140.8, 141.8, 144.8, 164.7, 165.6. ^{19}F NMR (565 MHz, DMSO-d_6) δ: 60.9. ESI−HRMS (*m/z*): [M − H]$^-$

calcd for $C_{20}H_{13}F_3N_2O_2$, 369.0856; obsd 369.0855.

4-((4'-(Trifluoromethyl)-[1,1'-biphenyl]-4-yl)amino)benzo[d]isoxazol-3-ol (6g). Flash column chromatography eluent: gradient from DCM/MeOH: 100/0 v/v to 98/2 v/v. White solid, m.p. = 227–228 °C dec (from diisopropyl ether/MeOH). Yield 80 %. ^{1}H-NMR (600 MHz, DMSO-d_6) δ 6.93 (d, $J = 8.1$ Hz, 1H), 7.01 (d, $J = 7.9$ Hz, 1H), 7.38–7.43 (m, 3H), 7.71 (d, $J = 8.3$ Hz, 2H), 7.77 (d, $J = 8.1$ Hz, 2H), 7.87 (d, $J = 8.0$ Hz, 2H), 8.09 (br s, 1H), 12.67 (very br s, 1H). ^{13}C-NMR (151 MHz, DMSO-d_6) δ 101.2, 104.0, 107.1, 119.8, 124.5 (d, $J = 271.6$ Hz), 125.7 (q, $J = 3.5$ Hz), 126.6, 127.1 (q, $J = 32.0$ Hz), 127.9, 131.5, 132.6, 139.5, 142.1, 143.8, 164.8, 165.6. ^{19}F NMR (565 MHz, DMSO-d_6) δ: 60.7. ESI−HRMS (*m/z*): [M − H]$^-$ calcd for $C_{20}H_{13}F_3N_2O_2$, 369.0856; obsd 369.0856.

4.3. Solubility assay at pH 7.4

Solubility was assayed in PBS as previously described [57]. Each solid compound (1 mg) was added to 1 mL of PBS (12 mM with NaCl 137 mM and KCl 2.7 mM, pH 7.4). The samples were shaken in an orbital shaker at 25 °C for 24 h, these suspensions were filtered through a PTFE 0.45 μm filter and the solutions were chromatographically analyzed using a Perkin Elmer UHPLC instrument, equipped with a reverse-phase (RP) C18 Phenomenex column (2.1 × 100 mm, 1.7 μm particle size). Solubility, expressed as μM concentration of the saturated solution, was calculated via interpolation with external calibration curves that were obtained with solutions of each compound in methanol.

4.4. Ionization and lipophilicity

Lipophilicity (LogD$^{7.4}$) was measured as previously described [32]. The ionization constants of the compounds were determined via potentiometric titration, as described in Ref. [32], while the spectrophotometric determination was measured according to Ref. [58].

4.5. AKR1C3 and AKR1C2 expression and purification

E.coli BL21 (DE) Codon Plus RP cells (Agilent Technologies) were transformed with the pGEX2T-modified plasmid that codes for either human AKR1C3 (H5Q) or C2 and that harbors a tobacco etch virus (TEV) protease recognition sequence, as previously described [30]. The expression and purification of both enzymes were performed as previously described [30]. Briefly, the bacteria cells were grown in YT2X media supplemented with ampicillin. Protein expression was induced by IPTG 0.5 mM for 3 h at 24 °C. The bacteria were then centrifuged and lysed in the presence of DNase, lysozyme and protease inhibitors. The lysate was centrifuged for 30 min at 13,000×g and the supernatant was collected. Proteins were affinity purified using N-terminal GST-tag on glutathione sepharose (GE-Healthcare), followed by His-tagged TEV protease digestion for GST-epitope removal. Then TEV protease was removed in a nickel-affinity chromatography step in 20 mM TRIS-HCl pH 8, 150 mM NaCl and 10 mM imidazole.

For MST analysis, a final size-exclusion chromatography step on a ENrich SEC 650 10 × 300 mm 24 ml column (GE Healthcare) was performed in 100 mM potassium phosphate buffer (pH 7.0) supplemented with 1 mM DTT.

4.6. Microscale thermophoresis (MST)

Microscale thermophoresis (MST) (Jerabek-Willemsen et al., 2014) experiments were carried out using a Monolith NT. 115 device (Nanotemper Technologies). A solution of purified AKR1C3 was labeled using the MO-L011 Monolith Protein Labeling Kit RED-NHS (Nanotemper Technologies). AKR1C3 was incubated at a concentration of 5 nM with serial dilutions of inhibitors (from 150 μM for compound **1** and 75 μM for compounds **6** and **6b**) in 100 mM potassium phosphate buffer (pH 7.0), supplemented with 100 μM NADP$^+$, 1 mM DTT, 5 % DMSO and

0.05 % Tween. Results were analyzed using GraphPad Prism Software. At least two experiments were performed for each interaction.

4.7. AKR1C3 and AKR1C2 inhibitor screening

The inhibition assays were performed on purified recombinant enzymes, as previously described [30]. Briefly, the enzymatic reaction was fluorimetrically (exc/em; 340 nm/460 nm) monitored via the measurement of NADPH production using an "Ensight" plate reader (Perkin Elmer) at 37 °C. The assay mixture, which contained S-tetralol (in EtOH), the inhibitor (in DMSO), 100 mM phosphate buffer pH 7, 200 μM NADP$^+$ and purified recombinant enzyme (0.4 μM), was added to a 96-well plate at a final volume of 200 μl with 4 % of EtOH and 6 % DMSO. The S-tetralol concentrations used in the AKR1C2 and AKR1C3 inhibition assays were 15 μM and 160 μM, respectively, in accordance with the Km described for the respective isoforms under the same experimental conditions. Percentage inhibition with respect to the controls, which contained the same amount of solvent without inhibitor, was calculated from the initial velocities, obtained via the linear regression of the progress curve at different inhibitor concentrations. The IC$_{50}$ values were obtained using GraphPad Prism. Results are expressed as mean value ± standard error (SE) of at least three experiments, each carried out in triplicate.

4.8. Cell lines

Human fetal lung fibroblast MRC-5 cells (ATCC) were cultured in EMEM supplemented with 10% (v/v) fetal bovine serum (FBS), 1 % non-essential amino acids (NEAA), 2 % (v/v) penicillin-streptomycin and 0.03 % L-glutamine. Prostate cancer 22RV1 cells (ATCC) were cultured in RPMI, supplemented with 10 % (v/v) FBS, 2 % (v/v) penicillin-streptomycin and 0.03 % L-glutamine. Both cell lines were grown at 37 °C in a humidified atmosphere containing 5 % CO$_2$. RPMI supplemented with 10% FBS, 1% L-glutamine and 1 % sodium pyruvate was used for LnCaP and the AKR1C3-transfected cell line variant. The latter was generated using a F279 V5 plasmid modified version of pIRES-P following protocol described in ref. [59].

4.9. Cell-proliferation assay

Cell-growth inhibition was evaluated using a sulforhodamine B colorimetric proliferation assay (SRB assay) modified by Vichai and Kirtikara, as previously described [30]. 10,000 cells/well were seeded into 96-well plates in the specific medium and incubated for 24 h. For the 22RV1 cells, a 10 % charcoal stripped serum (CSS) was used instead of FBS. Various dilutions of inhibitors in DMSO were then added in triplicate, and incubated for 72 h. Control cells were incubated with the same final concentration of DMSO (maximum concentration 1 % v/v). For the co-treatment experiments, 22RV1 cells were incubated for 72 h with ABI and either compound **6** or compound **6e** at the doses indicated above (from 2.5 μM to 20 μM). IC$_{50}$ values were obtained using GraphPad Prism Software. The values are the means of three separate experiments, each carried out in triplicate. The Enhancement Factor (EF) was calculated as:

$$EF = IC_{50}(ABI) / EC_{50}(\text{drug combination}).$$

4.10. Western blot

For the determination of PSA and AKR1C3 expression in PC cells, 300,000 cells/well were seeded into 6-well plates in the specific medium, which contained 10 % CSS, and incubated for 24 h. Two different dilutions of compounds **6** and **6e** in DMSO were then added to the wells and incubated for 72 h. Control cells were incubated with the same final

concentration of DMSO (maximum concentration 0.5 % v/v). Protein extraction from both untreated and treated cells was conducted using a RIPA lysis buffer containing the Complete Protease Inhibitor Cocktail (Roche Molecular Biochemicals). 30 μg of total protein lysate was loaded for western-blot analysis. For the detection of PSA and AKR1C3, rabbit anti-PSA 1:500 (sc-7316 Santa Cruz Biotechnology) and mouse anti-AKR1C3 1:5,000 (Sigma Aldrich) were used, respectively. The antibodies were added to the membrane and incubated overnight at 4 °C. The membrane was then washed and incubated with either HRP-conjugated secondary anti-mouse or anti-rabbit antibody 1:10,000 (Santa-Cruz Biotechnology), for 2 h at rt. Visualization was achieved using the chemiluminescent substrate Amersham ECL prime in the ChemiDoc Imaging System (Biorad). Rabbit anti-β-actin 1:1,000 (Cell Signaling Technology) was used as the internal control with overnight incubation at 4 °C.

4.11. Measurement of enzymatic activity of AKR1C3 in prostate cancer cells

Cells were seeded in 96-well plates in red phenol-free media and equilibrated at 37 °C in a 5 % CO_2 incubator overnight. Coumberone (MedChemEspress) was added to the plate at a concentration of 10 μM, reaching a final volume of 200 μl/well. Cells were incubated for a further 24 h. After transferring 100 μl of the supernatant into a 96-well black plate, the fluorescence intensity was read at excitation 355 nm and emission at 538 nm (cutoff 495 nm) using a Flexstation 3 Microplate Reader (Molecular Devices). The fluorescence intensity was normalized to the cell density obtained when performing the SRB assay (as above). The values are the average of three separate experiments each carried out in triplicate. Results were analyzed using GraphPad Prism Software and were deemed significant when $P \leq 0.05(*)$, $P \leq 0.01(**)$, $P \leq 0.001$ (***) and not significant with P values greater than 0.05.

4.12. Inhibition of the AKR1C3-mediated reduction of coumberone in 22RV1- and LNCaP-AKR1C3-transfected cells

Cells were added to 96-well plates in red phenol-free media at a density of 20,000 cells per well and incubated overnight at 37 °C in a 5 % CO_2 incubator. Cells were pre-treated with compounds **6**, **6e** and **6g** for 1-h, prior to the addition of coumberone (10 μM), reaching a final volume of 200 μl/well. After 24 h incubation, 100 μl of supernatant were transferred to a 96-well black plate and fluorescence intensity was measured (as above) and normalized to cell density using the SRB assay. Cells exposed to coumberone alone were considered to result in the maximum percentage (100 %) of coumberone reduction and consequently used as a reference. The values are the average of three separate experiments each carried out in triplicate. P values were calculated as reported above (4.11, measurement of enzymatic activity of AKR1C3 in prostate cancer cells).

4.13. Inhibition of AKR1C3-mediated testosterone production in 22RV1 cells using Elisa

22RV1 cells were seeded in 96-well plates in RPMI 6140 medium, supplemented with 10% charcoal-stripped serum, at a density of 30,000 cells per well. Cells were allowed to attach overnight. Compounds **6**, **6e** and **6g** were used at two concentrations to pre-treat cells for 1-h, prior to the addition of the testosterone precursor androstenedione (AD) (30 nM). Plates were returned to the incubator for a further 24 h. The cell supernatant was collected and diluted with Elisa Buffer (1:2) as per the manufacturer's guide for the Testosterone Elisa Kit (Cayman Chemical Company). The solution was then analyzed for testosterone detection using the above-mentioned kit. The color generated as a result of the reaction was quantified at a wavelength of 405 nm using a microplate reader. The concentration of testosterone was quantitated against a calibration curve generated using the ELISA buffer. Cells exposed to AD

alone were used as a reference. The values are the average of three separate experiments each carried out in triplicate. P values were calculated as reported above (4.11 measurement of enzymatic activity of AKR1C3 in prostate cancer cells).

4.14. Protein expression, purification and crystallization

The protein (AKR1C3) for crystallization was expressed and purified as previously described [31]. Fractions containing pure AKR1C3 were pooled and concentrated to 76.1 mg/mL, using a sample buffer consisting of 10 mM potassium phosphate pH 7, 1 mM EDTA and 1 mM DTT. AKR1C3 and the inhibitor **6b** were crystallized using the hanging vapor diffusion method. Both $NADP^+$ and inhibitor **6b** (dissolved in DMSO) were added at a final concentration of 2 mM to the protein solution (25 mg/mL) and incubated overnight at 6 °C (final concentration of DMSO <1%). For crystallization, 0.5 μL protein-ligand solution was mixed with 0.5 μL reservoir solution, and the plates were incubated at 6 °C. Crystals were observed within 1–2 weeks and appeared in 100 mM MES pH 6.0, 25% PEG 3350. The crystals were cryoprotected in the reservoir solution with 20 % ethylene glycol prior to the flash freezing of the crystals.

4.15. X-ray data collection, structure determination and refinement

X-ray diffraction data of the complex between AKR1C3, $NADP^+$ and **6b** were collected at MaxIV beamline Biomax, Lund, Sweden [60]. X-ray diffraction data were processed, scaled and merged using the auto-processing toolbox [61], which included XDS [62], as well as AIMLESS and POINTLESS in the CCP4 program suite [63]. The structure was determined via molecular replacement in Phaser [64], within the CCP4 program suite. The structure of AKR1C3 in complex with flufenamic acid (PDB-code 6f2u, chain A [31]) was used as the search model. The structure model was rebuilt using AutoBuild [65], within Phenix [66]. The structure was manually rebuilt in Coot [67], and refined using PHENIX. The atomic coordinates for inhibitor **6b** were created in Maestro (Maestro version 11.1; Schrödinger, LLC: New York, 2022) and subjected to the LigPrep procedure [68]. A restraint file for **6b** was generated using eLBOW [69], while maintaining the geometry from Maestro. TLS were applied during refinements. Individual *B*-factors were refined isotropically. *XYZ* (reciprocal) were refined. Translational pseudosymmetry (tNCS) is not included in refinements, as no significant change to R_{free} was observed. One loop region of the protein chain could not be modelled as electron density was very weak or absent, indicating a flexible loop (residue 131–136). At last, the structure was validated in the wwPDB OneDep [70] and figures were prepared in PyMol (The PyMOL Molecular Graphics System, Version 2.5.5, Schrödinger, LLC). Data-collection and refinement statistics are summarized in Table S5.

Data accessibility

The structure coordinates and corresponding structure factor files of the enzyme AKR1C3 in complex with $NADP^+$ and compound **6b** have been deposited in the Protein Data Bank (PDB) under the accession code (PDB ID: 8RB6).

CRediT authorship contribution statement

Agnese Chiara Pippione: Writing – review & editing, Writing – original draft, Investigation, Conceptualization. **Sandra Kovachka:** Investigation. **Chiara Vigato:** Investigation. **Laura Bertarini:** Writing – original draft, Investigation. **Iole Mannella:** Investigation. **Stefano Sainas:** Investigation. **Barbara Rolando:** Investigation. **Enrica Denasio:** Investigation. **Helen Piercy-Mycock:** Methodology. **Linda Romalho:** Investigation. **Edoardo Salladini:** Investigation. **Salvatore Adinolfi:** Investigation. **Daniele Zonari:** Methodology. **Caterina Peraldo-Neia:** Investigation. **Giovanna Chiorino:** Investigation. **Alice Passoni:** Investigation. **Osman Asghar Mirza:** Investigation. **Karla**

Frydenvang: Investigation. **Klaus Pors:** Validation, Investigation, Conceptualization. **Marco Lucio Lolli:** Writing – review & editing, Investigation. **Francesca Spyrakis:** Writing – review & editing, Writing – original draft, Investigation, Conceptualization. **Simonetta Oliaro-Bosso:** Writing – original draft, Supervision, Project administration, Investigation, Conceptualization. **Donatella Boschi:** Writing – review & editing, Writing – original draft, Supervision, Project administration, Conceptualization.

Declaration of competing interest

The authors declare that they have no known competing financial interests or personal relationships that could have appeared to influence the work reported in this paper.

Data availability

Data will be made available on request.

Abbreviations used

(AKR1C3) Aldo-keto reductase 1C3 isoform
(PC) prostate cancer
(ADT) androgen deprivation therapy
(CRPC) castration-resistant prostate cancer
(AR) androgen receptor
(FLU) flufenamic acid
(SP2) sub-pocket 2
(SP1) sub-pocket 1
(COX) cyclooxygenase
(AKR1C2) aldo-keto reductase 1C2 isoform
(DMSO-d_6) hexadeuterodimethyl sulfoxide
(CDCl3) deuterochloroform
(PSA) prostatic serum antigen
(rt) room temperature
(PBS) phosphate buffered saline
(CSS) charcoal stripped serum
(TFA) Trifluoroacetic acid
(THF) tetrahydrofuran
(DMF) dimethylformamide

Appendix A. Supplementary data

Supplementary data to this article can be found online at https://doi.org/10.1016/j.ejmech.2024.116193.

References

[1] C.M. Zeng, L.L. Chang, M.D. Ying, J. Cao, Q.J. He, H. Zhu, B. Yang, Aldo-keto reductase AKR1C1-AKR1C4: functions, regulation, and intervention for anti-cancer therapy, Front. Pharmacol. 8 (2017) 119.

[2] T.M. Penning, AKR1C3 (type 5 17beta-hydroxysteroid dehydrogenase/prostaglandin F synthase): roles in malignancy and endocrine disorders, Mol. Cell. Endocrinol. 489 (2019) 82–91.

[3] F. Meng, W.F. Li, D. Jung, C.C. Wang, T. Qi, C.S. Shia, R.Y. Hsu, Y.C. Hsieh, J. Duan, A novel selective AKR1C3-activated prodrug AST-3424/OBI-3424 exhibits broad anti-tumor activity, Am. J. Cancer Res. 11 (2021) 3645–3659.

[4] Y. Wang, Y. Liu, C. Zhou, C. Wang, N. Zhang, D. Cao, Q. Li, Z. Wang, An AKR1C3-specific prodrug with potent anti-tumor activities against T-ALL, Leuk. Lymphoma 61 (2020) 1660–1668.

[5] K. Evans, J. Duan, T. Pritchard, C.D. Jones, L. McDermott, Z. Gu, C.E. Toscan, N. El-Zein, C. Mayoh, S.W. Erickson, Y. Guo, F. Meng, D. Jung, K.S. Rathi, K.G. Roberts, C.G. Mullighan, C.-S. Shia, T. Pearce, B.A. Teicher, M.A. Smith, R.B. Lock, OBI-3424, a novel AKR1C3-activated prodrug, exhibits potent efficacy against preclinical models of T-ALL, Clin. Cancer Res. 25 (2019) 4493–4503.

[6] A.O. Adeniji, M. Chen, T.M. Penning, AKR1C3 as a target in castrate resistant prostate cancer, J. Steroid Biochem. Mol. Biol. 137 (2013) 136–149.

[7] O.O. Oduwole, Y. Li, V.V. Isomaa, A. Mäntyniemi, A.E. Pulkka, Y. Soini, P.T. Vihko, 17β-Hydroxysteroid dehydrogenase type 1 is an independent prognostic marker in breast cancer, Cancer Res. 64 (2004) 7604–7609.

[8] L. Xie, J. Yu, W. Guo, L. Wei, Y. Liu, X. Wang, X. Song, Aldo-keto reductase 1C3 may be a new radioresistance marker in non-small-cell lung cancer, Cancer Gene Ther. 20 (2013) 260–266.

[9] X. Li, X. Hong, X. Gao, X. Gu, W. Xiong, J. Zhao, H. Yu, M. Cui, M. Xie, Y. Bai, S. Sun, Methyl jasmonate enhances the radiation sensitivity of esophageal carcinoma cells by inhibiting the 11-ketoprostaglandin reductase activity of AKR1C3, Cancer Manag. Res. 10 (2018) 3149–3158.

[10] C. Zhou, Z. Wang, J. Li, X. Wu, N. Fan, D. Li, F. Liu, P.S. Plum, S. Hoppe, A. M. Hillmer, A. Quaas, F. Gebauer, S.-H. Chon, C.J. Bruns, Y. Zhao, Aldo-keto reductase 1C3 mediates chemotherapy resistance in esophageal adenocarcinoma via ROS detoxification, Cancers 13 (2021) 2403.

[11] D. Pan, W. Yang, Y. Zeng, H. Qin, Y. Xu, Y. Gui, X. Fan, G. Tian, Y. Wu, H. Sun, Y. Ye, S. Yang, J. Zhou, Q. Guo, L. Zhao, AKR1C3 regulated by NRF2/MAFG complex promotes proliferation via stabilizing PARP1 in hepatocellular carcinoma, Oncogene 41 (2022) 3846–3858.

[12] P. Zhu, R. Feng, X. Lu, Y. Liao, Z. Du, W. Zhai, K. Chen, Diagnostic and prognostic values of AKR1C3 and AKR1D1 in hepatocellular carcinoma, Aging 13 (2021) 4138–4156.

[13] D. Reddi, B.W. Seaton, D. Woolston, L. Aicher, L.D. Monroe, Z.J. Mao, J.C. Harrell, J.P. Radich, A. Advani, N. Papadantonakis, C.C.S. Yeung, AKR1C3 expression in T acute lymphoblastic leukemia/lymphoma for clinical use as a biomarker, Sci. Rep. 12 (2022) 5809.

[14] W. Xiong, J. Zhao, H. Yu, X. Li, S. Sun, Y. Li, Q. Xia, C. Zhang, Q. He, X. Gao, L. Zhang, D. Zhou, Elevated expression of AKR1C3 increases resistance of cancer cells to ionizing radiation via modulation of oxidative stress, PLoS One 9 (2014) e111911.

[15] S.Q. Sun, X. Gu, X.S. Gao, Y. Li, H. Yu, W. Xiong, H. Yu, W. Wang, Y. Li, Y. Teng, D. Zhou, Overexpression of AKR1C3 significantly enhances human prostate cancer cells resistance to radiation, Oncotarget 7 (2016) 48050–48058.

[16] C. Liu, W. Lou, Y. Zhu, J.C. Yang, N. Nadiminty, N.W. Gaikwad, C.P. Evans, A. C. Gao, Intracrine androgens and AKR1C3 activation confer resistance to Enzalutamide in Prostate Cancer, Cancer Res. 75 (2015) 1413–1422.

[17] A. Altavilla, C. Casadei, C. Lolli, C. Menna, G. Ravaglia, G. Gurioli, A. Farolfi, N. Brighi, V. Conteduca, S.L. Burgio, G. Schepisi, L. Rossi, S. Gargiulo, I. Lisotti, U. De Giorgi, Enzalutamide for the treatment of nonmetastatic castration-resistant prostate cancer, Expet Opin. Pharmacother. 21 (2020) 2091–2099.

[18] M.S. Litwin, H.J. Tan, The diagnosis and treatment of prostate cancer: a review, JAMA 317 (2017) 2532–2542.

[19] C. Liu, C.M. Armstrong, W. Lou, A. Lombard, C.P. Evans, A.C. Gao, Inhibition of AKR1C3 activation overcomes resistance to Abiraterone in advanced Prostate Cancer, Mol. Cancer Therapeut. 16 (2017) 35–44.

[20] K. Verma, N. Gupta, T. Zang, P. Wangtrakluldee, S.K. Srivastava, T.M. Penning, P. C. Trippier, AKR1C3 inhibitor KV-37 exhibits antineoplastic effects and potentiates enzalutamide in combination therapy in prostate adenocarcinoma cells, Mol. Cancer Therapeut. 17 (2018) 1833–1845.

[21] K. Verma, T. Zang, T.M. Penning, P.C. Trippier, Potent and highly selective aldo-keto reductase 1C3 (AKR1C3) inhibitors act as chemotherapeutic potentiators in acute myeloid leukemia and T-cell acute lymphoblastic leukemia, J. Med. Chem. 62 (2019) 3590–3616.

[22] J. Hofman, B. Malcekova, A. Skarka, E. Novotna, V. Wsol, Anthracycline resistance mediated by reductive metabolism in cancer cells: the role of aldo-keto reductase 1C3, Toxicol. Appl. Pharmacol. 278 (2014) 238–248.

[23] J. Chen, J. Zhang, W. Tian, C. Ge, Y. Su, J. Li, H. Tian, AKR1C3 suppresses ferroptosis in hepatocellular carcinoma through regulation of YAP/SLC7A11 signaling pathway, Mol. Carcinog. 62 (2023) 833–844.

[24] Y. Liu, S. He, Y. Chen, Y. Liu, F. Feng, W. Liu, Q. Guo, L. Zhao, H. Sun, Overview of AKR1C3: inhibitor achievements and disease insights, J. Med. Chem. 63 (2020) 11305–11329.

[25] T.M. Penning, Aldo-Keto Reductase (AKR) 1C3 inhibitors: a patent review, Expert Opin. Ther. Pat. 27 (2017) 1329–1340.

[26] T.L. Rizner, T.M. Penning, Aldo-keto reductase 1C3-Assessment as a new target for the treatment of endometriosis, Pharmacol. Res. 152 (2020) 104446.

[27] J.S. Choi, M.J. Jin, H.K. Han, Role of monocarboxylic acid transporters in the cellular uptake of NSAIDs, J. Pharm. Pharmacol. 57 (2005) 1185–1189.

[28] P. Lassalas, B. Gay, C. Lasfargeas, M.J. James, V. Tran, K.G. Vijayendran, K. R. Brunden, M.C. Kozlowski, C.J. Thomas, A.B. Smith 3rd, D.M. Huryn, C. Ballatore, Structure property relationships of carboxylic acid isosteres, J. Med. Chem. 59 (2016) 3183–3203.

[29] M.L. Lolli, I.M. Carnovale, A.C. Pippione, W.Y. Wahlgren, D. Bonanni, E. Marini, D. Zonari, M. Gallicchio, V. Boscaro, P. Goyal, R. Friemann, B. Rolando, R. Bagnati,

S. Adinolfi, S. Oliaro-Bosso, D. Boschi, Bioisosteres of indomethacin as inhibitors of aldo-keto reductase 1C3, ACS Med. Chem. Lett. 10 (2019) 437–443.

[30] A.C. Pippione, A. Giraudo, D. Bonanni, I.M. Carnovale, E. Marini, C. Cena, A. Costale, D. Zonari, K. Pors, M. Sadiq, D. Boschi, S. Oliaro-Bosso, M.L. Lolli, Hydroxytriazole derivatives as potent and selective aldo-keto reductase 1C3 (AKR1C3) inhibitors discovered by bioisosteric scaffold hopping approach, Eur. J. Med. Chem. 139 (2017) 936–946.

[31] A.C. Pippione, I.M. Carnovale, D. Bonanni, M. Sini, P. Goyal, E. Marini, K. Pors, S. Adinolfi, D. Zonari, C. Festuccia, W.Y. Wahlgren, R. Friemann, R. Bagnati, D. Boschi, S. Oliaro-Bosso, M.L. Lolli, Potent and selective aldo-keto reductase 1C3 (AKR1C3) inhibitors based on the benzoisoxazole moiety: application of a bioisosteric scaffold hopping approach to flufenamic acid, Eur. J. Med. Chem. 150 (2018) 930–945.

[32] A.C. Pippione, Z. Kilic-Kurt, S. Kovachka, S. Sainas, B. Rolando, E. Denasio, K. Pors, S. Adinolfi, D. Zonari, R. Bagnati, M.L. Lolli, F. Spyrakis, S. Oliaro-Bosso, D. Boschi, New aldo-keto reductase 1C3 (AKR1C3) inhibitors based on the hydroxytriazole scaffold, Eur. J. Med. Chem. 237 (2022) 114366.

[33] A.C. Pippione, S. Sainas, D. Boschi, M.L. Lolli, Hydroxyazoles as acid isosteres and their drug design applications—Part 2: bicyclic systems, in: Advances in Heterocyclic Chemistry, 2021.

[34] S. Sainas, A.C. Pippione, D. Boschi, M.L. Lolli, Hydroxyazoles as acid isosteres and their drug design applications—Part 1: monocyclic systems, in: Advances in Heterocyclic Chemistry, 2021.

[35] A.C. Pippione, D. Boschi, K. Pors, S. Oliaro-Bosso, M.L. Lolli, Androgen-AR axis in primary and metastatic prostate cancer: chasing steroidogenic enzymes for therapeutic intervention, J Cancer Metastasis Treat 3 (2017) 328–361.

[36] Y. Amano, T. Yamaguchi, T. Niimi, H. Sakashita, Structures of complexes of type 5 17β-hydroxysteroid dehydrogenase with structurally diverse inhibitors: insights into the conformational changes upon inhibitor binding, Acta Crystallogr D Biol Crystallogr 71 (2015) 918–927.

[37] M.K. Dahlgren, P. Schyman, J. Tirado-Rives, W.L. Jorgensen, Characterization of biaryl torsional energetics and its treatment in OPLS all-atom force fields, J. Chem. Inf. Model. 53 (2013) 1191–1199.

[38] M.P. Johansson, J. Olsen, Torsional barriers and equilibrium angle of biphenyl: reconciling theory with experiment, J. Chem. Theor. Comput. 4 (2008) 1460–1471.

[39] D.W. Widlicka, J.C. Murray, K.J. Coffman, C.G. Xiao, M.A. Brodney, J.P. Rainville, B. Samas, Two routes to 4-Fluorobenzisoxazol-3-one in the synthesis of a 5-HT partial agonist, Org. Process Res. Dev. 20 (2016) 233–241.

[40] K.C. Nicolaou, C.R. Hale, C. Nilewski, H.A. Ioannidou, A. ElMarrouni, L. G. Nilewski, K. Beabout, T.T. Wang, Y. Shamoo, Total synthesis of viridicatumtoxin B and analogues thereof: strategy evolution, structural revision, and biological evaluation, J. Am. Chem. Soc. 136 (2014) 12137–12160.

[41] A. Kikuchi, T. Furutani, H. Azami, K. Watanabe, T. Niimi, Y. Kamiyama, S. Kuromitsu, E. Baskin-Bey, M. Heeringa, T. Ouatas, K. Enjo, In vitro and in vivo characterisation of ASP9521: a novel, selective, orally bioavailable inhibitor of 17βHSD5; AKR1C3), Invest. N. Drugs 32 (2014) 860–870.

[42] C.W. Murray, D.A. Erlanson, A.L. Hopkins, G.M. Keseru, P.D. Leeson, D.C. Rees, C. H. Reynolds, N.J. Richmond, Validity of ligand efficiency metrics, ACS Med. Chem. Lett. 5 (2014) 616–618.

[43] T.W. Johnson, R.A. Gallego, M.P. Edwards, Lipophilic efficiency as an important metric in drug design, J. Med. Chem. 61 (2018) 6401–6420.

[44] G. Motyan, M.K. Gopisetty, R.E. Kiss-Faludy, A. Kulmany, I. Zupko, E. Frank, M. Kiricsi, Anti-cancer activity of novel dihydrotestosterone-derived ring A-condensed pyrazoles on androgen non-responsive prostate cancer cell lines, Int. J. Mol. Sci. 20 (2019).

[45] J.V. Jovankic, D.D. Nikodijevic, M.G. Milutinovic, A.G. Nikezic, V.V. Kojic, A. M. Cvetkovic, D.M. Cvetkovic, Potential of Orlistat to induce apoptotic and antiangiogenic effects as well as inhibition of fatty acid synthesis in breast cancer cells, Eur. J. Pharmacol. 939 (2023) 175456.

[46] S. Endo, H. Oguri, J. Segawa, M. Kawai, D. Hu, S. Xia, T. Okada, K. Irie, S. Fujii, H. Gouda, K. Iguchi, T. Matsukawa, N. Fujimoto, T. Nakayama, N. Toyooka, T. Matsunaga, A. Ikari, Development of novel AKR1C3 inhibitors as new potential treatment for castration-resistant prostate cancer, J. Med. Chem. 63 (2020) 10396–10411.

[47] T.M. Wrobel, K. Sharma, I. Mannella, S. Oliaro-Bosso, P. Nieckarz, T. Du Toit, C. D. Voegel, M.N. Rojas Velazquez, J. Yakubu, A. Matveeva, S. Therkelsen, F. S. Jorgensen, A.V. Pandey, A.C. Pippione, M.L. Lolli, D. Boschi, F. Bjorkling, Exploring the potential of sulfur moieties in compounds inhibiting steroidogenesis, Biomolecules 13 (2023) 1349–1367.

[48] S.M. Jamieson, Y. Gu, D.M. Manesh, J. El-Hoss, D. Jing, K.L. Mackenzie, C.P. Guise, A. Foehrenbacher, S.M. Pullen, J. Benito, J.B. Smaill, A.V. Patterson, M.A. Mulaw, M. Konopleva, S.K. Bohlander, R.B. Lock, W.R. Wilson, A novel fluorometric assay for aldo-keto reductase 1C3 predicts metabolic activation of the nitrogen mustard prodrug PR-104A in human leukaemia cells, Biochem. Pharmacol. 88 (2014) 36–45.

[49] F. Milletti, L. Storchi, G. Sforna, S. Cross, G. Cruciani, Tautomer enumeration and stability prediction for virtual screening on large chemical databases, J. Chem. Inf. Model. 49 (2009) 68–75.

[50] A.C. Pippione, F. Dosio, A. Ducime, A. Federico, K. Martina, S. Sainas, B. Frolund, M. Gooyit, K.D. Janda, D. Boschi, M.L. Lolli, Substituted 4-hydroxy-1,2,3-triazoles: synthesis, characterization and first drug design applications through bioisosteric

[51] S. Sainas, P. Temperini, J.C. Farnsworth, F. Yi, S. Mollerud, A.A. Jensen, B. Nielsen, A. Passoni, J.S. Kastrup, K.B. Hansen, D. Boschi, D.S. Pickering, R.P. Clausen, M. L. Lolli, Use of the 4-hydroxytriazole moiety as a bioisosteric tool in the development of ionotropic glutamate receptor ligands, J. Med. Chem. 62 (2019) 4467–4482.

[52] R. Farid, T. Day, R.A. Friesner, R.A. Pearlstein, New insights about HERG blockade obtained from protein modeling, potential energy mapping, and docking studies, Bioorg. Med. Chem. 14 (2006) 3160–3173.

[53] W. Sherman, T. Day, M.P. Jacobson, R.A. Friesner, R. Farid, Novel procedure for modeling ligand/receptor induced fit effects, J. Med. Chem. 49 (2006) 534–553.

[54] W. Sherman, H.S. Beard, R. Farid, Use of an induced fit receptor structure in virtual screening, Chem. Biol. Drug Des. 67 (2006) 83–84.

[55] R.A. Friesner, R.B. Murphy, M.P. Repasky, L.L. Frye, J.R. Greenwood, T.A. Halgren, P.C. Sanschagrin, D.T. Mainz, Extra precision glide: docking and scoring incorporating a model of hydrophobic enclosure for protein-ligand complexes, J. Med. Chem. 49 (2006) 6177–6196.

[56] E. Rubin, A.C. Pippione, M. Boyko, G. Einaudi, S. Sainas, M. Collino, C. Cifani, M. L. Lolli, N. Abu-Freha, J. Kaplanski, D. Boschi, A.N. Azab, A new NF-kappaB inhibitor, MEDS-23, reduces the severity of adverse post-ischemic stroke outcomes in rats, Brain Sci. 12 (2021) 35–51.

[57] S. Sainas, M. Giorgis, P. Circosta, G. Poli, M. Alberti, A. Passoni, V. Gaidano, A. C. Pippione, N. Vitale, D. Bonanni, B. Rolando, A. Cignetti, C. Ramondetti, A. Lanno, D.M. Ferraris, B. Canepa, B. Buccinna, M. Piccinini, M. Rizzi, G. Saglio, S. Al-Karadaghi, D. Boschi, R. Miggiano, T. Tuccinardi, M.L. Lolli, Targeting acute myelogenous leukemia using potent human dihydroorotate dehydrogenase inhibitors based on the 2-Hydroxypyrazolo[1,5-a]pyridine scaffold: SAR of the aryloxyaryl moiety, J. Med. Chem. 65 (2022) 12701–12724.

[58] A. Albert, E.P. Serjeant, Ionization Constants of Acids and Bases, A Laboratory Manual, Methuen, 1962.

[59] C.P. Guise, M.R. Abbattista, R.S. Singleton, S.D. Holford, J. Connolly, G.U. Dachs, S.B. Fox, R. Pollock, J. Harvey, P. Guilford, F. Donate, W.R. Wilson, A.V. Patterson, The bioreductive prodrug PR-104A is activated under aerobic conditions by human aldo-keto reductase 1C3, Cancer Res. 70 (2010) 1573–1584.

[60] T. Ursby, K. Ahnberg, R. Appio, O. Aurelius, A. Barczyk, A. Bartalesi, M. Bjelcic, F. Bolmsten, Y. Cerenius, R.B. Doak, M. Eguiraun, T. Eriksson, R.J. Friel, I. Gorgisyan, A. Gross, V. Haghighat, F. Hennies, E. Jagudin, B. Norsk Jensen, T. Jeppsson, M. Kloos, J. Lidon-Simon, G.M.A. de Lima, R. Lizatovic, M. Lundin, A. Milan-Otero, M. Milas, J. Nan, A. Nardella, A. Rosborg, A. Shilova, R. L. Shoeman, F. Siewert, P. Sondhauss, V.O. Talibov, H. Tarawneh, J. Thanell, M. Thunnisen, J. Unge, C. Ward, A. Gonzalez, U. Mueller, BioMAX - the first macromolecular crystallography beamline at MAX IV Laboratory, J. Synchrotron Radiat. 27 (2020) 1415–1429.

[61] C. Vonrhein, C. Flensburg, P. Keller, A. Sharff, O. Smart, W. Paciorek, T. Womack, G. Bricogne, Data processing and analysis with the autoPROC toolbox, Acta Crystallogr D Biol Crystallogr 67 (2011) 293–302.

[62] W. Kabsch, Xds, Acta Crystallogr D Biol Crystallogr 66 (2010) 125–132.

[63] M.D. Winn, C.C. Ballard, K.D. Cowtan, E.J. Dodson, P. Emsley, P.R. Evans, R. M. Keegan, E.B. Krissinel, A.G. Leslie, A. McCoy, S.J. McNicholas, G.N. Murshudov, N.S. Pannu, E.A. Potterton, H.R. Powell, R.J. Read, A. Vagin, K.S. Wilson, Overview of the CCP4 suite and current developments, Acta Crystallogr D Biol Crystallogr 67 (2011) 235–242.

[64] A.J. McCoy, R.W. Grosse-Kunstleve, P.D. Adams, M.D. Winn, L.C. Storoni, R. J. Read, Phaser crystallographic software, J. Appl. Crystallogr. 40 (2007) 658–674.

[65] T.C. Terwilliger, R.W. Grosse-Kunstleve, P.V. Afonine, N.W. Moriarty, P.H. Zwart, L.W. Hung, R.J. Read, P.D. Adams, Iterative model building, structure refinement and density modification with the PHENIX AutoBuild wizard, Acta Crystallogr D Biol Crystallogr 64 (2008) 61–69.

[66] D. Liebschner, P.V. Afonine, M.L. Baker, G. Bunkóczi, V.B. Chen, T.I. Croll, B. Hintze, L.W. Hung, S. Jain, A.J. McCoy, N.W. Moriarty, R.D. Oeffner, B.K. Poon, M.G. Prisant, R.J. Read, J.S. Richardson, D.C. Richardson, M.D. Sammito, O. V. Sobolev, D.H. Stockwell, T.C. Terwilliger, A.G. Urzhumtsev, L.L. Videau, C. J. Williams, P.D. Adams, Macromolecular structure determination using X-rays, neutrons and electrons: recent developments in Phenix, Acta Crystallogr D Struct Biol 75 (2019) 861–877.

[67] P. Emsley, B. Lohkamp, W.G. Scott, K. Cowtan, Features and development of Coot, Acta Crystallogr D Biol Crystallogr 66 (2010) 486–501.

[68] G.M. Sastry, M. Adzhigirey, T. Day, R. Annabhimoju, W. Sherman, Protein and ligand preparation: parameters, protocols, and influence on virtual screening enrichments, J. Comput. Aided Mol. Des. 27 (2013) 221–234.

[69] N.W. Moriarty, R.W. Grosse-Kunstleve, P.D. Adams, Electronic Ligand Builder and Optimization Workbench (eLBOW): a tool for ligand coordinate and restraint generation, Acta Crystallogr D Biol Crystallogr 65 (2009) 1074–1080.

[70] J.Y. Young, J.D. Westbrook, Z. Feng, R. Sala, E. Peisach, T.J. Oldfield, S. Sen, A. Gutmanas, D.R. Armstrong, J.M. Berrisford, L. Chen, M. Chen, L. Di Costanzo, D. Dimitropoulos, G. Gao, S. Ghosh, S. Gore, V. Guranovic, P.M.S. Hendrickx, B. P. Hudson, R. Igarashi, Y. Ikegawa, N. Kobayashi, C.L. Lawson, Y. Liang, S. Mading, L. Mak, M.S. Mir, A. Mukhopadhyay, A. Patwardhan, I. Persikova, L. Rinaldi, E. Sanz-Garcia, M.R. Sekharan, C. Shao, G.J. Swaminathan, L. Tan, E.L. Ulrich, G. van Ginkel, R. Yamashita, H. Yang, M.A. Zhuravleva, M. Quesada, G. J. Kleywegt, H.M. Berman, J.L. Markley, H. Nakamura, S. Velankar, S.K. Burley, OneDep: unified wwPDB system for deposition, biocuration, and validation of macromolecular structures in the PDB archive, Structure 25 (2017) 536–545.